copurified along with proteins with known chromatin and epigenetic functions (Figure 3). Among them were PARP1 and components of NuRD, Swi/Snf-like BAF, and PcG complexes (Figure 3B). Indeed, knockdown of PARP1, BAF53a (Swi/Snf-like BAF complex), and CHD4 (NuRD complex) resulted in derepression of HO-1 (Figures 6A and 6C). Since these proteins are known to repress the expression of target genes as corepressors of transcription and/or remodeling factors of chromatin architecture (Brand et al., 2004, Wacker et al., 2007), these proteins, together with MATIIα, may also participate in target gene repression by MafK and Bach1 (Figure 7J).

MATIIβ is known to inhibit the catalytic activity of MATIIα by sensitizing it to the product inhibition by SAM (LeGros et al., 2001). We found that MATIIβ was recruited to the MafK target genes and required for their repression, indicating that MATIIβ is a stimulatory rather than inhibitory subunit of MATIIα in terms of transcription regulation. Recently, it has been reported that splicing variants of MATIIβ are present in nuclei and interact with mRNA binding protein HuR (Xia et al., 2010). Although its relevance to transcription regulation is not clear at present and we did not detect HuR in our proteomics analyses, this finding also supports nuclear function of MATIIβ. Since β-like subunit is not found in MATI/III, molecular function of MATIIβ on chromatin will be an important issue.

Considering that MATIIα and -β were present in a high-molecular-mass fraction with CHD4 and BAF53a, and that this particular form coupled SAM synthesis and histone methylation in vitro (Figure 7I), the core of this form, MATIIα and MATIIβ, was named the SAMIT module. "Module" is used to reflect our observations that MATIIβ was also critical for the corepressor activity and that they further interacted with chromatin regulators and histone H1 and H3 methyltransferase activities (Figure 7J). The interaction of methyltransferase activities with SAMIT module suggests that SAM produced by MATIIα in situ may be utilized to inhibit MafK/Bach1 target genes. Whereas the catalytically inactive MATIIα interfered with HO-1 repression, exogenous SAM failed to reverse the effect of MATIIα knockdown (Figures 5D and 5E). These observations support the notion that the catalytic function of MATIIα plays a role at sites of recruitment. SAM may be utilized for methylation of protein(s) (Figure 7J). One possible target may be dimethylation of H3K4 and K9, which can potentially inhibit transcription via regulation of histone acetylation and remodeling on euchromatic regions (Figures 5A–5C; Kim and Buratowski, 2009; Fritsch et al., 2010). While we identified G9a, Ehmt1, and ALL1/KMT2A methyltransferases upon the single-step purification of MATIIα (Figure 3), we did not detect them in the further purified SAMIT module (Figure 7H) by immunoblotting analysis (data not shown). Thus, the interaction of MATIIα with G9a and ALL1 may be dynamic. Identification of the methyltransferase activities copurified with SAMIT is now underway.

The list of MATIIα-associated proteins suggests functions of MATIIα and SAMIT beyond MafK. The presence of DNA-binding transcription factors such as GATA1 and Runx1 in the MATII-associating proteins (Figure 3) raises the possibility that these transcription factors may utilize MATIIα/SAMIT as a coregulator as well. Several Polycomb-related proteins were found in the purified MATIIα fraction, being consistent with the genetic interaction with Polycomb in *Drosophila melanogaster* (Larsson et al., 1996).

Regulation of metabolic flux by enzyme compartmentalization is a well-established concept. The presence of MATIIα in nuclear compartment may allow efficient coupling of SAM synthesis and methylation of target protein or DNA by methyltransferases. Considering that SAM is an energetically precious but labile molecule generated in the expense of ATP, its production in situ may allow fine and efficient tuning of the cascade reactions for histone and DNA methylation. The list of MATIIα-associating proteins will be helpful to foster integrative understanding of chromatin-based regulations.

## EXPERIMENTAL PROCEDURES

### Plasmids

pOZ-N-MafK plasmid was described previously (Ochiai et al., 2006). Construction of MATIIα expression plasmid is described in the Supplemental Experimental Procedures.

### Immunohistochemistry

Basic indirect immunofluorescence of paraformaldehyde-fixed cells was described previously (Francastel et al., 2001). All processes are described in the Supplemental Experimental Procedures.

### MafK and MATIIα Complex Purification and Mass Spectrometric Analysis

MafK complex purification was carried out as previously described from X63/0 cells expressing eMafK (Ochiai et al., 2006). FLBio-tagged protein purification was carried out as previously described (de Boer et al., 2003). Each protein was determined using LC-HCT plus (Bruker Daltonics) or LTQ (Thermo Fisher Scientific), and MASCOT search engine (Matrix Science). Glycerol gradient sedimentation was carried out as previously described (Dohi et al., 2008) and also described in the Supplemental Experimental Procedures.

### RNA Interference

Stealth RNAi duplexes were designed to target MATIIα and β, MafK, BAF53a, CHD4, and PARP1 using the BLOCK-iT RNAi Designer (Invitrogen Corporation, Carlsbad, CA). All RNAi sequences are described in the Supplemental Experimental Procedures.

### ChIP and ChPD Analysis

ChIP and ChPD were performed as described previously (Sawado et al., 2001; de Boer et al., 2003). Anti-methylated H3K4 and H3K9, and anti-acetylated H3K9 and H3K27 antibodies were described previously (Kimura et al., 2008). The enrichment of the DNA template was analyzed and quantified by semi-quantitive PCR using primers as described in the Supplemental Experimental Procedures. Relative enrichment was calculated as the difference between specific antibody and normal IgG signals (ChIP), or as that of FLBio-MATIIα or FLBio-MafK and BirA signals (ChPD) normalized to the respective input signals.

### In Vitro HMT and MAT-HMT Assay

In vitro HMT assays were performed as described previously (Tachibana et al., 2001). In vitro MAT-dependent HMT (MAT-HMT) assays were carried out by modifying in vitro HMT assay. All processes are described in the Supplemental Experimental Procedures.

## SUPPLEMENTAL INFORMATION

Supplemental Information includes Supplemental Experimental Procedures, Supplemental References, six figures, and two tables and can be found with this article at doi:10.1016/j.molcel.2011.02.018.

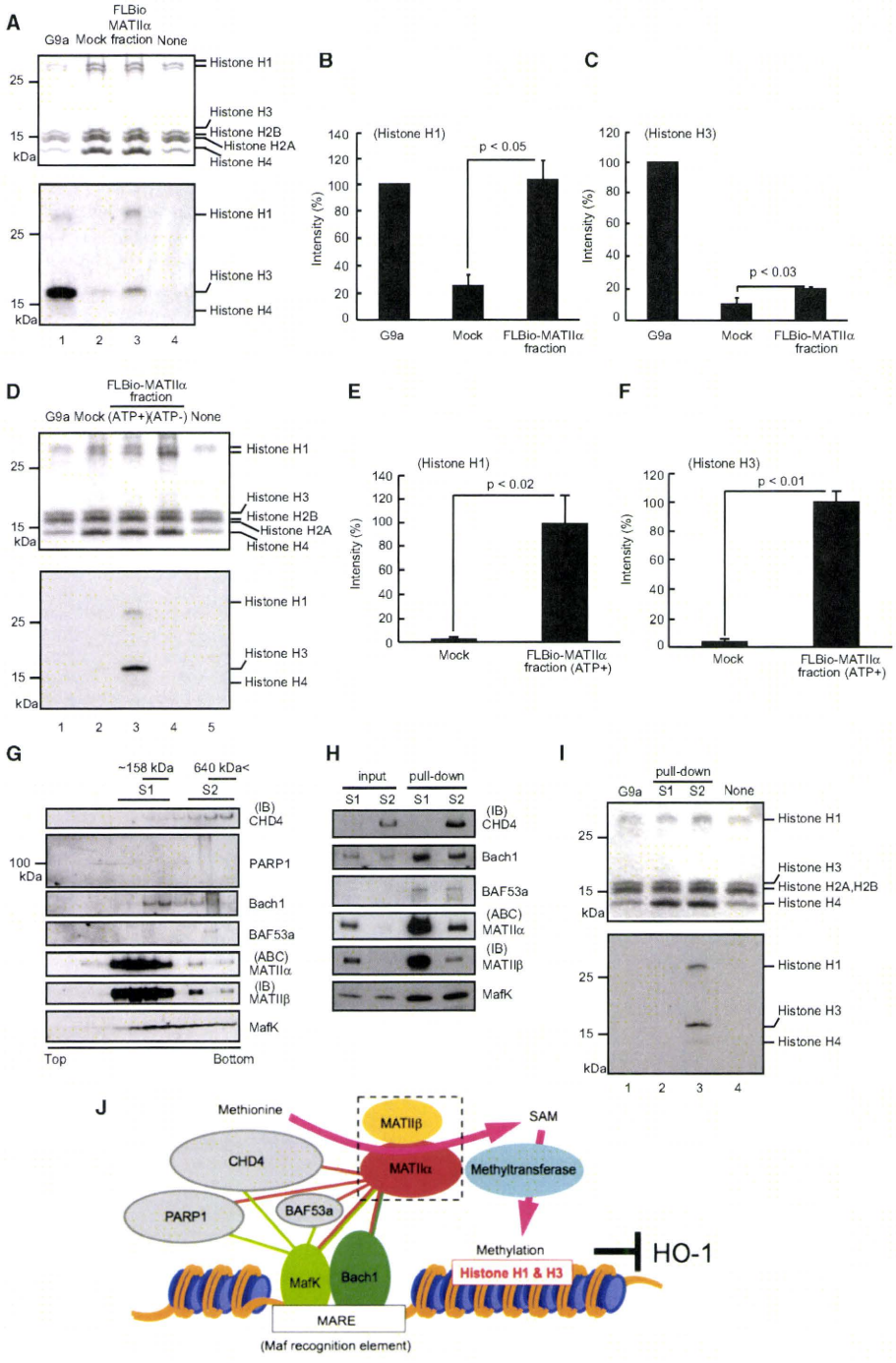


**Figure 7. Interaction of Methyltransferase Activity with MATIIα**

(A) HMT assays were carried out with recombinant GST-G9a (lane 1), affinity-purified fractions of control cells (mock; lane 2) or MATIIα cells (FLBio-MATIIα; lane 3) using avidin beads, or no protein added (none; lane 4). CBB staining (top panel) and fluorography (bottom panel) are shown.

## ACKNOWLEDGMENTS

We thank Dr. H. Motohashi (Tohoku University) for critical reading of the manuscript and comments; C. Teruya (Tohoku University) for mass spectrometric analysis; Drs. K. Itoh, A. Maruyama (Hirosaki University), J. Sharif, Y. Dohi, A. Muto, K. Murayama (Tohoku University), and M. Matsumoto and K. Nakayama (Kyusyu University) for discussion and help; Dr. H. Kimura (Osaka University) for antibodies to methylated H3K4 and H3K9, and acetylated H3K9 and H3K27; and Dr. M. Tachibana (Kyoto University) for HMT assay protocol. The biotin tag system was kindly provided by Dr. A.B. Cantor (Children's Hospital Boston). This work was supported by Grants-in-aid from the Ministry of Education, Science, Sport, and Culture of Japan, grant from the Naito Foundation for Research on "Nuclear Dynamics and RNA," grant from the Nukada scholarship, Toho University, and global COE program for Network Medicine, Tohoku University. Part of this study was supported by Biomedical Research Core of Tohoku University School of Medicine.

Received: November 6, 2009
Revised: August 18, 2010
Accepted: December 22, 2010
Published: March 3, 2011

## REFERENCES

Andrews, N.C., Erdjument-Bromage, H., Davidson, M.B., Tempst, P., and Orkin, S.H. (1993). Erythroid transcription factor NF-E2 is a haematopoietic-specific basic-leucine zipper protein. Nature *362*, 722–728.

Brand, M., Ranish, J.A., Kummer, N.T., Hamilton, J., Igarashi, K., Francastel, C., Chi, T.H., Crabtree, G.R., Aebersold, R., and Groudine, M. (2004). Dynamic changes in transcription factor complexes during erythroid differentiation revealed by quantitative proteomics. Nat. Struct. Mol. Biol. *11*, 73–80.

Chamberlin, M.E., Ubagai, T., Pao, V.Y., Pearlstein, R.A., and Chou, J.Y. (2000). Structural requirements for catalysis and dimerization of human methionine adenosyltransferase I/III. Arch. Biochem. Biophys. *373*, 56–62.

de Boer, E., Rodriguez, P., Bonte, E., Krijgsveld, J., Katsantoni, E., Heck, A., Grosveld, F., and Strouboulis, J. (2003). Efficient biotinylation and single-step purification of tagged transcription factors in mammalian cells and transgenic mice. Proc. Natl. Acad. Sci. USA *100*, 7480–7485.

Dillon, S.C., Zhang, X., Trievel, R.C., and Cheng, X. (2005). The SET-domain protein superfamily: protein lysine methyltransferases. Genome Biol. *6*, 227.

Dohi, Y., Ikura, T., Hoshikawa, Y., Katoh, Y., Ota, K., Nakanome, A., Muto, A., Omura, S., Ohta, T., Ito, A., et al. (2008). Bach1 inhibits oxidative stress-induced cellular senescence by impeding p53 function on chromatin. Nat. Struct. Mol. Biol. *15*, 1246–1254.

Francastel, C., Magis, W., and Groudine, M. (2001). Nuclear relocation of a transactivator subunit precedes target gene activation. Proc. Natl. Acad. Sci. USA *98*, 12120–12125.

Fritsch, L., Robin, P., Mathieu, J.R., Souidi, M., Hinaux, H., Rougeulle, C., Harel-Bellan, A., Ameyar-Zazoua, M., and Ait-Si-Ali, S. (2010). A subset of the histone H3 lysine 9 methyltransferases Suv39h1, G9a, GLP, and SETDB1 participate in a multimeric complex. Mol. Cell *37*, 46–56.

Fujiwara, K.T., Kataoka, K., and Nishizawa, M. (1993). Two new members of the maf oncogene family, mafK and mafF, encode nuclear b-Zip proteins lacking putative trans-activator domain. Oncogene *8*, 2371–2380.

Goll, M.G., and Bestor, T.H. (2005). Eukaryotic cytosine methyltransferases. Annu. Rev. Biochem. *74*, 481–514.

Halim, A.B., LeGros, L., Chamberlin, M.E., Geller, A., and Kotb, M. (2001). Regulation of the human MAT2A gene encoding the catalytic alpha 2 subunit of methionine adenosyltransferase, MAT II: gene organization, promoter characterization, and identification of a site in the proximal promoter that is essential for its activity. J. Biol. Chem. *276*, 9784–9791.

Hall, D.A., Zhu, X., Royce, T., Gerstein, M., and Snyder, M. (2004). Regulation of gene expression by a metabolic enzyme. Science *306*, 482–484.

Hintze, K.J., Katoh, Y., Igarashi, K., and Theil, E.C. (2007). Bach1 repression of ferritin and thioredoxin reductase1 is heme-sensitive in cells and in vitro and coordinates expression with heme oxygenase1, beta-globin, and NADP(H) quinone (oxido) reductase1. J. Biol. Chem. *282*, 34365–34371.

Igarashi, K., and Sun, J. (2006). The heme-Bach1 pathway in the regulation of oxidative stress response and erythroid differentiation. Antioxid. Redox Signal. *8*, 107–118.

Igarashi, K., Kataoka, K., Itoh, K., Hayashi, N., Nishizawa, M., and Yamamoto, M. (1994). Regulation of transcription by dimerization of erythroid factor NF-E2 p45 with small Maf proteins. Nature *367*, 568–572.

Igarashi, K., Itoh, K., Motohashi, H., Hayashi, N., Matuzaki, Y., Nakauchi, H., Nishizawa, M., and Yamamoto, M. (1995). Activity and expression of murine small Maf family protein MafK. J. Biol. Chem. *270*, 7615–7624.

Ishii, T., Itoh, K., Takahashi, S., Sato, H., Yanagawa, T., Katoh, Y., Bannai, S., and Yamamoto, M. (2000). Transcription factor Nrf2 coordinately regulates a group of oxidative stress-inducible genes in macrophages. J. Biol. Chem. *275*, 16023–16029.

Itoh, K., Chiba, T., Takahashi, S., Ishii, T., Igarashi, K., Katoh, Y., Oyake, T., Hayashi, N., Satoh, K., Hatayama, I., et al. (1997). An Nrf2/small Maf heterodimer mediates the induction of phase II detoxifying enzyme genes through antioxidant response elements. Biochem. Biophys. Res. Commun. *236*, 313–322.

Kataoka, K., Igarashi, K., Itoh, K., Fujiwara, K.T., Noda, M., Yamamoto, M., and Nishizawa, M. (1995). Small Maf proteins heterodimerize with Fos and may act as competitive repressors of the NF-E2 transcription factor. Mol. Cell. Biol. *15*, 2180–2190.

Keyse, S.M., and Tyrrell, R.M. (1989). Heme oxygenase is the major 32-kDa stress protein induced in human skin fibroblasts by UVA radiation, hydrogen peroxide, and sodium arsenite. Proc. Natl. Acad. Sci. USA *86*, 99–103.

Kim, T., and Buratowski, S. (2009). Dimethylation of H3K4 by Set1 recruits the Set3 histone deacetylase complex to 5′ transcribed regions. Cell *137*, 259–272.

Kimura, H., Hayashi-Takanaka, Y., Goto, Y., Takizawa, N., and Nozaki, N. (2008). The organization of histone H3 modifications as revealed by a panel of specific monoclonal antibodies. Cell Struct. Funct. *33*, 61–73.

(B and C) Relative levels of methylation of histone H1 (B) and H3 (C) are shown. The methylation level of histones by GST-G9a was arbitrarily set at 100%. These results represent three independent experiments with standard deviation.
(D) MAT-HMT assays were carried out using ATP and labeled methionine as in (A). ATP was omitted in lane 4.
(E and F) Relative levels of methylation of histone H1 (E) and H3 (F) in (D) are shown. The methylation level of histones by MATIIα fraction was arbitrarily set at 100%. These results represent three independent experiments with standard deviation.
(G–I) FLBio-MATIIα was purified using FLAG antibody and then separated with glycerol gradient centrifugation. Fractions were analyzed with indicated antibodies (G). FLBio-MATIIα was further affinity purified from the pooled fractions (S1 and S2 in G) using biotin-avidin and analyzed as above (H). MAT-HMT assay with recombinant GST-G9a or the purified MATIIα complex from S1 or S2 were carried out (I). Reaction mixtures alone were used as a control (none; lane 4). CBB-stained gel (top) and fluorography (bottom) are shown, representing three independent studies.
(J) A model for MATII function. Copurified proteins are connected with lines whose colors indicate tagged bait proteins. MATIIα functions as a corepressor of MafK-Bach1 by locally providing SAM and forming SAMIT module with MATIIβ (dashed line). SAM may be used for methylation required for repression including histone H1 and H3 such as H3K4 and K9 me2.

Kotb, M., Mudd, S.H., Mato, J.M., Geller, A.M., Kredich, N.M., Chou, J.Y., and Cantoni, G.L. (1997). Consensus nomenclature for the mammalian methionine adenosyltransferase genes and gene products. Trends Genet. *13*, 51–52.

Larsson, J., Zhang, J., and Rasmuson-Lestander, A. (1996). Mutations in the Drosophila melanogaster gene encoding S-adenosylmethionine synthetase suppress position-effect variegation. Genetics *143*, 887–896.

LeGros, L., Halim, A.B., Chamberlin, M.E., Geller, A., and Kotb, M. (2001). Regulation of the human MAT2B gene encoding the regulatory beta subunit of methionine adenosyltransferase, MAT II. J. Biol. Chem. *276*, 24918–24924.

Lu, S.C., and Mato, J.M. (2008). S-Adenosylmethionine in cell growth, apoptosis and liver cancer. J. Gastroenterol. Hepatol. *23* (*Suppl 1*), S73–S77.

Motohashi, H., Katsuoka, F., Shavit, J.A., Engel, J.D., and Yamamoto, M. (2000). Positive or negative MARE-dependent transcriptional regulation is determined by the abundance of small Maf proteins. Cell *103*, 865–875.

Muto, A., Hoshino, H., Madisen, L., Yanai, N., Obinata, M., Karasuyama, H., Hayashi, N., Nakauchi, H., Yamamoto, M., Groudine, M., and Igarashi, K. (1998). Identification of Bach2 as a B-cell-specific partner for small maf proteins that negatively regulate the immunoglobulin heavy chain gene 3′ enhancer. EMBO J. *17*, 5734–5743.

Muto, A., Tashiro, S., Nakajima, O., Hoshino, H., Takahashi, S., Sakoda, E., Ikebe, D., Yamamoto, M., and Igarashi, K. (2004). The transcriptional programme of antibody class switching involves the repressor Bach2. Nature *429*, 566–571.

Ochiai, K., Katoh, Y., Ikura, T., Hoshikawa, Y., Noda, T., Karasuyama, H., Tashiro, S., Muto, A., and Igarashi, K. (2006). Plasmacytic transcription factor Blimp-1 is repressed by Bach2 in B cells. J. Biol. Chem. *281*, 38226–38234.

Ochiai, K., Muto, A., Tanaka, H., Takahashi, S., and Igarashi, K. (2008). Regulation of the plasma cell transcription factor Blimp-1 gene by Bach2 and Bcl6. Int. Immunol. *20*, 453–460.

Oyake, T., Itoh, K., Motohashi, H., Hayashi, N., Hoshino, H., Nishizawa, M., Yamamoto, M., and Igarashi, K. (1996). Bach proteins belong to a novel family of BTB-basic leucine zipper transcription factors that interact with MafK and regulate transcription through the NF-E2 site. Mol. Cell. Biol. *16*, 6083–6095.

Reytor, E., Pérez-Miguelsanz, J., Alvarez, L., Pérez-Sala, D., and Pajares, M.A. (2009). Conformational signals in the C-terminal domain of methionine adenosyltransferase I/III determine its nucleocytoplasmic distribution. FASEB J. *23*, 3347–3360.

Sakata, S.F., Shelly, L.L., Ruppert, S., Schutz, G., and Chou, J.Y. (1993). Cloning and expression of murine S-adenosylmethionine synthetase. J. Biol. Chem. *268*, 13978–13986.

Sakata, S.F., Okumura, S., Matsuda, K., Horikawa, Y., Maeda, M., Kawasaki, K., Chou, J.Y., and Tamaki, N. (2005). Effect of fasting on methionine adenosyltransferase expression and the methionine cycle in the mouse liver. J. Nutr. Sci. Vitaminol. (Tokyo) *51*, 118–123.

Sawado, T., Igarashi, K., and Groudine, M. (2001). Activation of β-major globin gene transcription is associated with recruitment of NF-E2 to the β-globin LCR and gene promoter. Proc. Natl. Acad. Sci. USA *98*, 10226–10231.

Shi, Y. (2007). Histone lysine demethylases: emerging roles in development, physiology and disease. Nat. Rev. Genet. *8*, 829–833.

Sun, J., Hoshino, H., Takaku, K., Nakajima, O., Muto, A., Suzuki, H., Tashiro, S., Takahashi, S., Shibahara, S., Alam, J., et al. (2002). Hemoprotein Bach1 regulates enhancer availability of heme oxygenase-1 gene. EMBO J. *21*, 5216–5224.

Sun, J., Brand, M., Zenke, Y., Tashiro, S., Groudine, M., and Igarashi, K. (2004). Heme regulates the dynamic exchange of Bach1 and NF-E2-related factors in the Maf transcription factor network. Proc. Natl. Acad. Sci. USA *101*, 1461–1466.

Tachibana, M., Sugimoto, K., Fukushima, T., and Shinkai, Y. (2001). Set domain-containing protein, G9a, is a novel lysine-preferring mammalian histone methyltransferase with hyperactivity and specific selectivity to lysines 9 and 27 of histone H3. J. Biol. Chem. *276*, 25309–25317.

Tahara, T., Sun, J., Igarashi, K., and Taketani, S. (2004a). Heme-dependent up-regulation of the alpha-globin gene expression by transcriptional repressor Bach1 in erythroid cells. Biochem. Biophys. Res. Commun. *324*, 77–85.

Tahara, T., Sun, J., Nakanishi, K., Yamamoto, M., Mori, H., Saito, T., Fujita, H., Igarashi, K., and Taketani, S. (2004b). Heme positively regulates the expression of beta-globin at the locus control region via the transcriptional factor Bach1 in erythroid cells. J. Biol. Chem. *279*, 5480–5487.

Takahashi, H., McCaffery, J.M., Irizarry, R.A., and Boeke, J.D. (2006). Nucleocytosolic acetyl-coenzyme a synthetase is required for histone acetylation and global transcription. Mol. Cell *23*, 207–217.

Wacker, D.A., Ruhl, D.D., Balagamwala, E.H., Hope, K.M., Zhang, T., and Kraus, W.L. (2007). The DNA binding and catalytic domains of poly(ADP-ribose) polymerase 1 cooperate in the regulation of chromatin structure and transcription. Mol. Cell. Biol. *27*, 7475–7485.

Wellen, K.E., Hatzivassiliou, G., Sachdeva, U.M., Bui, T.V., Cross, J.R., and Thompson, C.B. (2009). ATP-citrate lyase links cellular metabolism to histone acetylation. Science *324*, 1076–1080.

Xia, M., Chen, Y., Wang, L.C., Zandi, E., Yang, H., Bemanian, S., Martinez-Chantar, M.L., Mato, J.M., and Lu, S.C. (2010). Novel function and intracellular localization of methionine adenosyltransferase 2 beta splicing variants. J. Biol. Chem. *285*, 20015–20021.

Zhang, J., Ohta, T., Maruyama, A., Hosoya, T., Nishikawa, K., Maher, J.M., Shibahara, S., Itoh, K., and Yamamoto, M. (2006). BRG1 interacts with Nrf2 to selectively mediate HO-1 induction in response to oxidative stress. Mol. Cell. Biol. *26*, 7942–7952.

# LETTER

doi:10.1038/nature09574

# Transcriptional activation of polycomb-repressed genes by ZRF1

Holger Richly[1], Luciana Rocha-Viegas[1], Joana Domingues Ribeiro[1], Santiago Demajo[1], Gunes Gundem[2], Nuria Lopez-Bigas[2], Tekeya Nakagawa[3], Sabine Rospert[4], Takashi Ito[3] & Luciano Di Croce[1,5]

**Covalent modification of histones is fundamental in orchestrating chromatin dynamics and transcription[1–3]. One example of such an epigenetic mark is the mono-ubiquitination of histones, which mainly occurs at histone H2A and H2B[4–6]. Ubiquitination of histone H2A has been implicated in polycomb-mediated transcriptional silencing[7–9]. However, the precise role of the ubiquitin mark during silencing is still elusive. Here we show in human cell lines that ZRF1 (zuotin-related factor 1) is specifically recruited to histone H2A when it is ubiquitinated at Lys 119 by means of a novel ubiquitin-interacting domain that is located in the evolutionarily conserved zuotin domain. At the onset of differentiation, ZRF1 specifically displaces polycomb-repressive complex 1 (PRC1) from chromatin and facilitates transcriptional activation. A genome-wide mapping of ZRF1, RING1B and H2A-ubiquitin targets revealed its involvement in the regulation of a large set of polycomb target genes, emphasizing the key role ZRF1 has in cell fate decisions. We provide here a model of the molecular mechanism of switching polycomb-repressed genes to an active state.**

To identify proteins capable of binding ubiquitinated H2A (H2Aub), we developed an affinity purification based on the expression of Flag-tagged histone H2A. Among several potential H2Aub-binding proteins (Supplementary Fig. 1A, C and Supplementary Table 1), we chose to analyse ZRF1 in more depth, as within its carboxy terminus this protein contains two SANT domains, which are often found in subunits of chromatin-remodelling complexes (Fig. 1a). Intriguingly, its yeast homologue Zuo1 is linked to the ubiquitination of histone H2B in *Saccharomyces cerevisae*[10]. Moreover, ZRF1 has also been implicated in cancer and differentiation[11–13]. It adopts an oligomeric conformation and is located in the nucleus as well as in the cytosol (Supplementary Figs 1D, E and 2A). Purification of mononucleosomes from 293T cells expressing Flag-tagged histone H2A, either wild type or mutated (KKRR) at the ubiquitination sites (K118/K119), revealed ubiquitin-specific ZRF1 binding preferentially to the wild-type mononucleosomes (Fig. 1b and Supplementary Fig. 1B, F, H, I). Corroborating this finding, we observed specific binding of ubiquitinated wild-type nucleosomes to recombinant ZRF1 (Fig. 1c). Thus, these data point to the ubiquitin mark at histone H2A as a docking site for ZRF1.

ZRF1 shares homology in the zuotin domain with its yeast orthologue Zuo1 (Fig. 1a), which is synthetically lethal with Rad6, the E2 enzyme involved in the specific ubiquitination of histone H2B[10]. We reasoned that the conserved zuotin domain might contain the ubiquitin-binding motif[14]. Results from pull-down experiments with a GST–ubiquitin fusion protein and different recombinant ZRF1 truncation proteins allowed us to map the ubiquitin-binding domain (UBD) to a region C-terminal of the DnaJ domain (Fig. 1d). H2A ubiquitination as well as histone H3K27me3 are marks typically located in promoter regions of polycomb-silenced genes[15,16]. To test for ubiquitin-dependent recruitment of ZRF1 to chromatin, we established NT2 knockdown cell lines for ZRF1 or RING1B (a PRC1 subunit that is an E3 ligase; Fig. 1e). We then analysed occupancy at several promoter regions of polycomb-repressed genes, including *PER1*, *NF1C* (Fig. 1f) and the well-characterized *HOX* genes[15,16]. ZRF1 enrichment at the promoters clearly depended on the abundance of RING1B and on H2Aub levels (Fig. 1g, h and Supplementary Fig. 1G).

It has been shown that PRC1 is tethered to chromatin by the interaction of its subunit PC1 with a trimethyl mark on Lys 27 of histone H3 (H3K27me3)[8,16]. Using purified mononucleosomes containing either wild-type H2A or the H2A(KKRR) mutant, we observed that co-purification of the PRC1 subunits RING1B and BMI1 depended on the ubiquitination of histone H2A (Fig. 2a). In contrast, we did not find an alteration of the H3K27 methylation levels in nucleosomes devoid of the ubiquitin mark, indicating that stable maintenance of PRC1 at chromatin depends on the ubiquitin mark (Fig. 2a and Supplementary Fig. 2J). To understand the functional relationship between ZRF1 and PRC1, we characterized further the binding affinity of RING1B towards the ubiquitin residue by GST pull-down experiments (Supplementary Fig. 2B). Furthermore, after reconstituting RING1B-containing mononucleosome complexes, RING1B was efficiently released from nucleosomes following incubation with GST–ubiquitin (Fig. 2b and Supplementary Fig. 2C). This finding indicated that ZRF1 could compete with RING1B for binding at H2Aub. Indeed, ZRF1 overexpression led to displacement of the PRC1 subunits RING1B and BMI1 from chromatin, whereas ZRF1 knockdown led to an enhanced occupancy of RING1B at chromatin that caused an increase in H2A ubiquitination (Fig. 2c, d and Supplementary Fig. 2D–H). We next performed competition assays with the GST–ubiquitin substrate. When the His-tagged RING1B concentration was maintained, we observed that increasing the His–ZRF1 concentration led to a reduction of RING1B bound to the ubiquitin substrate, emphasizing the competition for the ubiquitin residue by both proteins (Fig. 2e). We then assembled recombinant RING1B–GST–ubiquitin complexes and performed pull-down experiments after adding either bovine serum albumin (BSA) alone (lane 1) or recombinant His–UBD and BSA (lanes 2 and 3). In concordance with the previous result, we observed RING1B replaced by the UBD of ZRF1 (Fig. 2f). Similarly, on reconstituted RING1B–mononucleosome complexes, ZRF1 efficiently displaced RING1B (Fig. 2g and Supplementary Fig. 2I). Finally, chromatin immunoprecipitation (ChIP) experiments in 293T cells overexpressing either ZRF1 or only the UBD, indicated an enrichment of ZRF1 or the UBD at promoters of the *HOX* gene cluster concomitantly with the displacement of the PRC1 subunits RING1B and BMI1 (Fig. 2h–i and Supplementary Fig. 2F). In contrast, neither a ZRF1 deletion mutant devoid of the UBD nor the yeast homologue Zuo1, which shows only a weak ubiquitin-binding capacity, were recruited to chromatin or were able to displace PRC1 (Supplementary Fig. 3A–C). It has been shown that depletion of RING1B, and thus H2A ubiquitination, leads to the loss of PRC2 from chromatin[17]. In agreement with this previous study, we found that PRC2 levels were reduced at KKRR mutant nucleosomes.

[1]Centre de Regulació Genòmica (CRG)/UPF, 08003 Barcelona, Spain. [2]Department of Experimental and Health Sciences, Universitat Pompeu Fabra, 08003 Barcelona, Spain. [3]Nagasaki University School of Medicine, Nagasaki 852-8523, Japan. [4]Institut für Biochemie und Molekularbiologie (ZBMZ), Universität Freiburg, 79104 Germany. [5]Institució Catalana de Recerca i Estudis Avançats (ICREA), Centre de Regulació Genòmica (CRG), PRBB, c/ Dr. Aiguader 88, 08003 Barcelona, Spain.

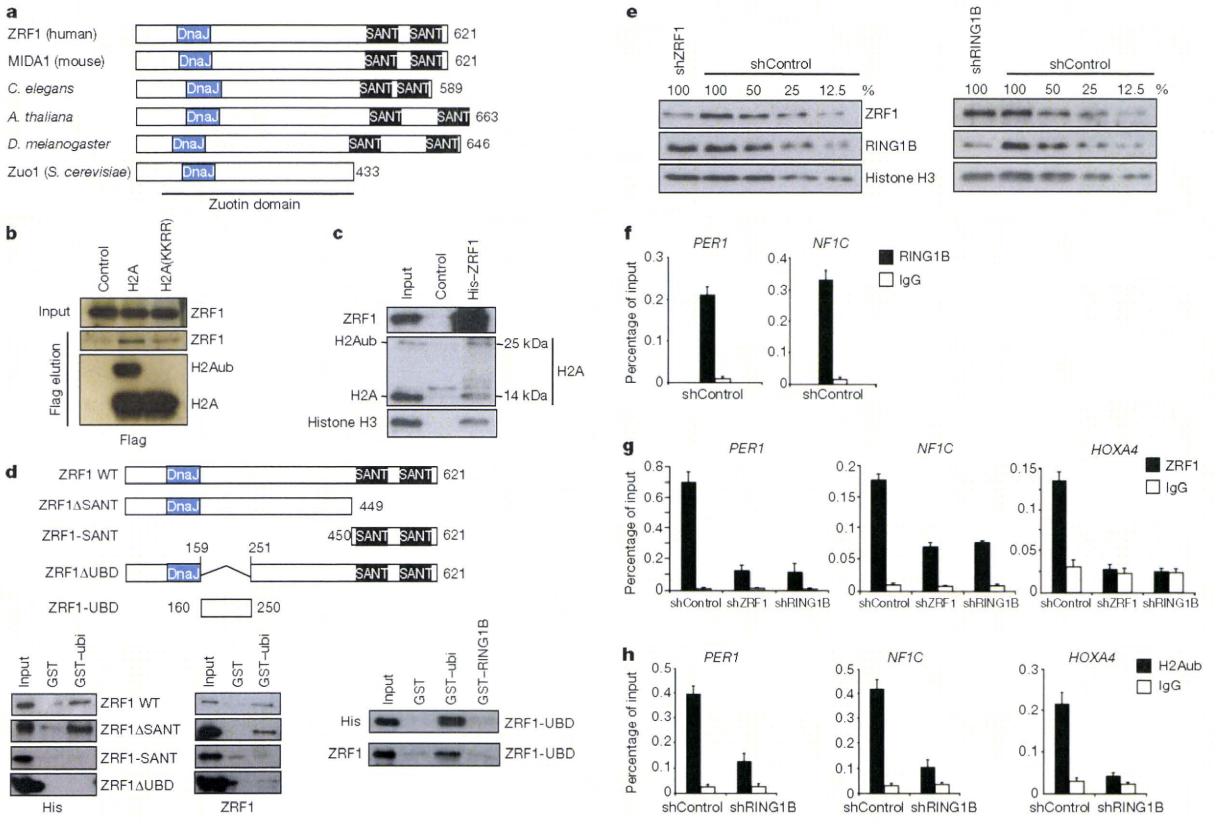


**Figure 1 | ZRF1 interacts with H2Aub.** **a**, Schematic diagram of ZRF1 orthologues indicating the DnaJ domain and SANT domains. The numbers along the right-hand side of panels **a** and **d** refer to the number of amino acids each of the proteins is composed of. **b**, Flag-tagged histone H2A and H2A(KKRR) were expressed in 293T cells. Mononucleosomes were purified and eluates were subjected to immunoblot analysis using ZRF1 and Flag antibodies. The inputs correspond to 3%. **c**, Nuclear protein extracts containing mononucleosomes were incubated with recombinant His–ZRF1. Precipitated ZRF1–nucleosome complexes were subjected to immunoblot analysis using the indicated antibodies. The inputs represent 5% of His–ZRF1 and 2% of the protein extract. **d**, GST pull-downs with GST, GST–ubiquitin (GST–ubi) and GST–RING1B (right panel) and the His-tagged proteins indicated. Bound material was subjected to immunoblot analysis using His and ZRF1 antibodies. The input shown represents 2%. WT, wild type. **e**, Protein extracts of RING1B and ZRF1 knockdown cell lines were subjected to immunoblotting and probed with the antibodies indicated in the figure. **f**, ChIP experiments performed in NT2 control cells with RING1B antibodies. **g**, **h**, ChIP experiments performed in the NT2 control and knockdown cells with ZRF1 and H2Aub antibodies. The occupancy at promoters of the *PER1*, *NF1C* and *HOXA4* genes was tested by quantitative PCR. Data are represented as mean ± s.e.m. ($n = 3$).

Similarly, PRC2 levels decreased upon binding of ZRF1 to chromatin (Supplementary Fig. 4A–C).

To globally identify ZRF1 target genes, we performed a ChIP-on-chip (see Methods) analysis in NT2 cells[18,19]. Because our data indicate that ZRF1 might antagonize silencing by polycomb proteins, we designed an experiment that allowed us to study the occupancy of ZRF1 under conditions of retinoic-acid-induced differentiation (Fig. 3a). We found ZRF1 to be enriched in 758 (not induced), 2,295 (induced for 1 h) or 995 (induced for 3 h) genes (Fig. 3b and Supplementary Table 2). Analysis of the ZRF1 occupancy at its target genes revealed a marked increase at 1 h of induction (Fig. 3b, Supplementary Fig. 5C and Supplementary Table 2). Clustering the target genes with respect to their cellular functions indicates a role for ZRF1 in developmental processes and differentiation (Fig. 3c, d and Supplementary Fig. 5A, B). Additional ChIP-on-chip analysis indicates that RING1B and H2Aub target genes are mainly involved in developmental processes (Supplementary Figs 7A–L, 8A–J and Supplementary Tables 4 and 5), as shown in previous publications[20,21]. The overlap of ZRF1 targets (1 h retinoic acid) with RING1B and H2Aub targets led to the identification of 1,102 common target genes (Fig. 3e, f). Moreover, comparison of ZRF1 target genes with polycomb target genes[22] indicates that ZRF1 is more closely linked to PRC1 than to PRC2 (Supplementary Figs 6A, B, 8K, L). We next performed a gene expression analysis comparing short hairpin RNA targeting *ZRF1* (shZRF1) with shControl (non-specific shRNA constructs) cells, with or without retinoic-acid treatment. Interestingly, downregulated genes in shZRF1 after retinoic-acid stimulation are ZRF1 or polycomb targets, particularly for PRC1 and H2Aub (Supplementary Figs 6C, 9A–G and Supplementary Table 6). Among these genes more than a hundred are targeted by ZRF1, RING1B and H2Aub and many of these are major players in developmental pathways (Fig. 4a, b). To corroborate our findings, we performed ChIP experiments and gene expression analysis on selected ZRF1 target genes. We found that ZRF1 was significantly enriched at these genes only after stimulation with retinoic acid (Fig. 4c and Supplementary Fig. 10A). Under the same conditions, we observed transcriptional activation of the same genes in wild-type NT2 cells. However, in ZRF1 knockdown cells, we detected a decrease of the messenger RNA levels (Fig. 4d and Supplementary Fig. 10B). In sum, the data presented show a clear involvement of ZRF1 in the PRC1 pathway and, most importantly, that activation of genes targeted by PRC1 and H2Aub is facilitated by ZRF1.

Several polycomb target genes become activated during differentiation, concomitantly with the disappearance of the polycomb-dependent repressive marks[15,16,23,24]. Analysis of two *HOXA* genes revealed that retinoic-acid-induced transcriptional activation depended on the presence of ZRF1. In contrast, RING1B knockdown caused a more robust

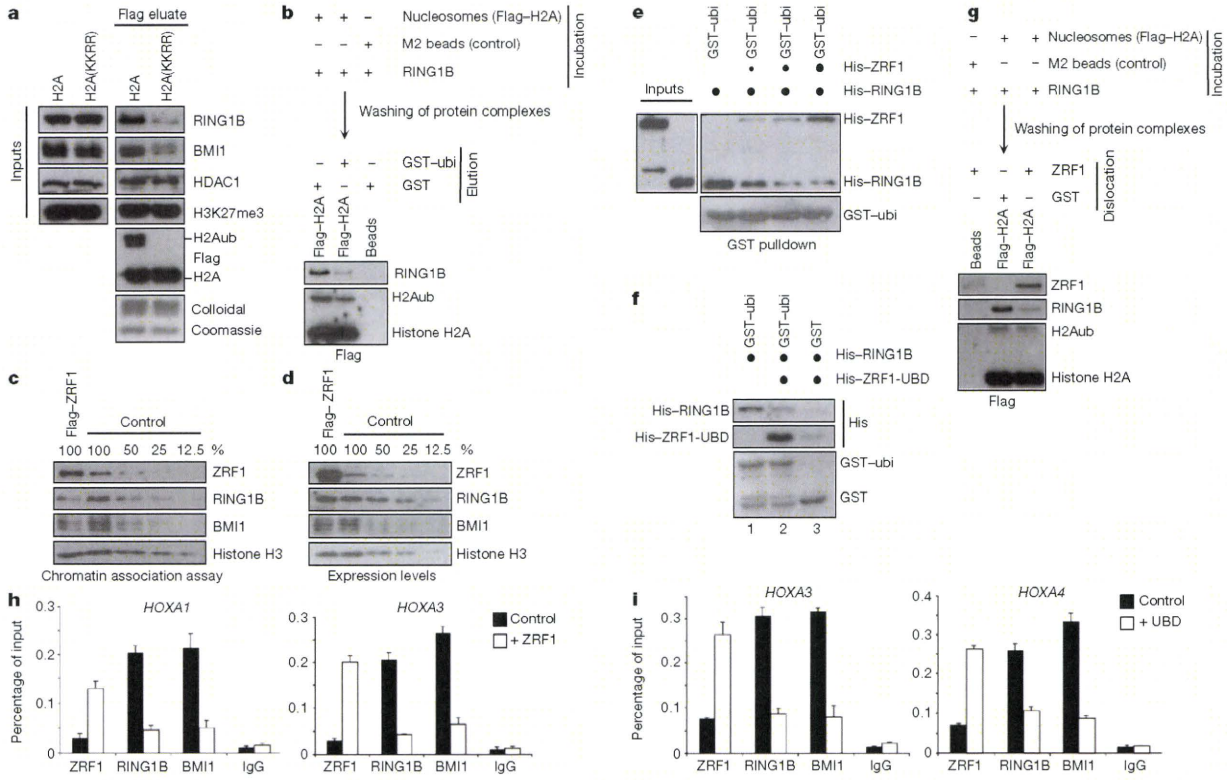


**Figure 2 | ZRF1 and PRC1 compete for binding of H2Aub.**
**a**, Mononucleosomes were purified from 293T cells expressing Flag-tagged H2A or a double mutant (KKRR). The purified material was subjected to immunoblot analysis using the indicated antibodies. The inputs represent 3%. **b**, Nucleosome–His–RING1B complexes were assembled, washed and incubated with GST (70 ng $\mu l^{-1}$) or GST–ubiquitin (70 ng $\mu l^{-1}$). Flag eluates were subjected to immunoblot analysis with the indicated antibodies. **c**, Chromatin association assay of 293T cells overexpressing ZRF1. Immunoblot analysis was performed with the indicated antibodies. **d**, Immunoblot analysis of 293T cells overexpressing ZRF1 using the indicated antibodies. **e**, GST–ubiquitin was incubated with constant amounts of His–RING1B and increasing amounts of His–ZRF1 finally reaching equimolar levels (last lane). The inputs show 10% of His–RING1B and 10% of the maximal amount of His–ZRF1. **f**, GST and GST–ubiquitin were incubated with RING1B, washed and incubated with His–ZRF1-UBD (see Methods). The retained material was subjected to immunoblot analysis with His antibodies. Lane 1 shows the pull-down in the presence of only BSA, lanes 2 and 3 in the presence of both BSA and His–ZRF1-UBD. **g**, Nucleosome–His–RING1B complexes were assembled and incubated with GST (100 ng $\mu l^{-1}$) or ZRF1 (100 ng $\mu l^{-1}$). After elution by Flag peptide, immunoblot analysis was performed with Flag, RING1B and ZRF1 antibodies. **h**, ChIP experiments with ZRF1, RING1B and BMI1 antibodies after overexpression of ZRF1 in 293T cells. **i**, Experiments were performed as already stated with the exception that the Flag–UBD was overexpressed instead of the full-length ZRF1. The occupancy at promoters of *HOX* genes was tested with quantitative PCR. Data are represented as mean ± s.e.m. ($n = 3$).

activation of those genes, thus supporting opposing roles for PRC1 and ZRF1 in transcriptional regulation of promoters (Fig. 4e). Next we investigated the occupancy of both ZRF1 and RING1B at promoters of *HOX* genes during retinoic-acid-induced transcription. Retinoic-acid treatment led to the recruitment of ZRF1 to promoter regions with a concomitant reduction of RING1B occupancy, clearly indicating mutually exclusive binding for these proteins at chromatin (Fig. 4f, g). Accordingly, in ZRF1 knockdown cells, RING1B was not efficiently removed from chromatin after retinoic-acid induction (Fig. 4h), as supported by previous experiments (Fig. 2a–h). In related experiments (1 h retinoic acid) we found H2Aub to be slightly reduced at *HOXA* gene promoters, indicating a deletion of this histone mark shortly after the removal of PRC1 complexes (Supplementary Fig. 11A–C). A set of similar results was obtained in retinoic-acid-induced differentiation of leukaemic cells (Supplementary Fig. 10C–E)[24]. On the basis of our results, we reasoned that ZRF1 might facilitate transcription. Recently, it has been shown that USP21-mediated H2A deubiquitination precedes gene activation[25]. To investigate further the impact of ZRF1 on transcriptional activation, we performed *in vitro* experiments testing whether ZRF1 might act in concert with specific deubiquitinases. *In vitro* deubiquitination assays carried out with mouse liver chromatin demonstrate that ZRF1 facilitates H2A deubiquitination (Fig. 4i). Thus, these results showed that, besides its function in the displacement of PRC1 complexes, ZRF1 facilitates transcription by cooperating with deubiquitinase enzymes.

Ubiquitination of H2A has long been correlated with activation of genes[26]. It is intriguing that ubiquitination of histone H2A not only has an effect on gene silencing but also is necessary to attract a factor that switches genes from a silenced to a transcriptionally activated state. However, it is still unclear how ZRF1 binding to chromatin is regulated (Supplementary Fig. 12A, B). One potential mode of regulating ZRF1, and thus cell differentiation, could be to mask its UBD domain. It has been shown that proteins of the ID (inhibitor of differentiation) family bind to ZRF1 in a region spanning its UBD domain[13] (Supplementary Fig. 12C). Our data indicate that association of PRC1 with chromatin depends on the H2Aub mark, whereas H3K27me3 is not sufficient to retain PRC1 complexes and is most probably required for its initial targeting[21,27]. RING1B/PRC1 are not as abundant as H2Aub, thus excluding a continuous binding of PRC1 complexes throughout chromatin. Yet it has been shown that during DNA damage H2A E3 ligases bind ubiquitinated H2A and propagate the initial chromatin ubiquitination marks[28]. A similar sliding mechanism could also apply to our findings regarding RING1B, and challenge the current view of ubiquitination and deubiquitination cycles (see also Supplementary

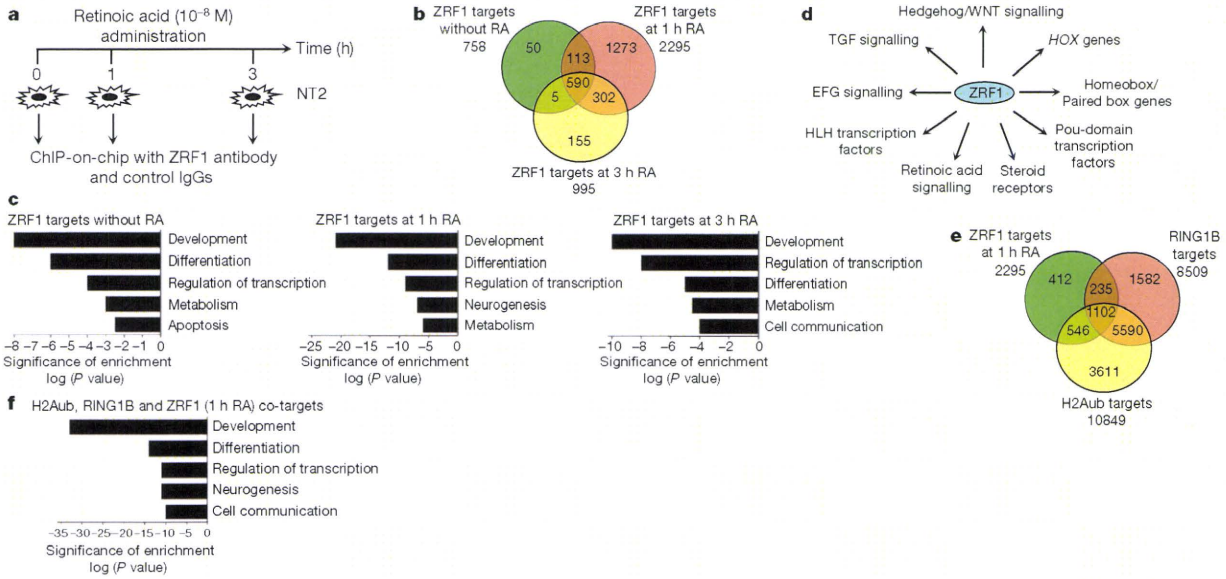


**Figure 3 | Genome-wide mapping of ZRF1 target genes in NT2 cells.** **a**, Schematic representation of the experimental approach for the ChIP-on-chip experiment. Chromatin was subjected to triplicate ChIP experiments with ZRF1 and control antibodies. The obtained material was amplified and hybridized with Human Promoter Arrays chips from Agilent. **b**, Venn diagram of the ZRF1 target genes as obtained by Chipper analysis. **c**, Functional enrichment analysis of ZRF1 target genes at the different time points of retinoic-acid (RA) induction. **d**, A selection of ZRF1 target genes identified in this study (induced for 1 h), focusing on those known to be involved in key pathways controlling cell fate decisions. **e**, Venn diagram showing significant overlapping between the gene lists of RING1B, H2Aub and ZRF1 (induced for 1 h) as obtained by ChIP-on-chip analysis. The *P* values after overlapping the H2Aub target genes with ZRF1 and/or RING1B targets are listed in the following: RING1B ($P = 10^{-16}$), ZRF1 (1 h; $P = 10^{-12}$) and RING1B-ZRF1 co-targets ($P = 10^{-16}$). **f**, Functional enrichment analysis of the 1,102 common ZRF1/RING1B/H2Aub target genes.

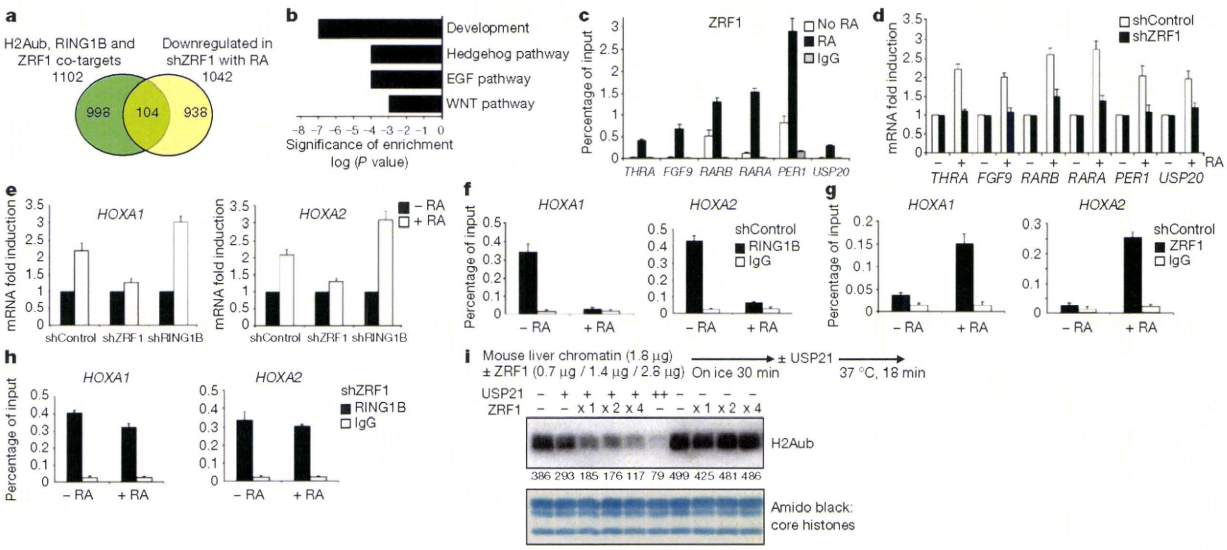


**Figure 4 | ZRF1 functions in activating polycomb-repressed genes.** **a**, The list of genes significantly repressed in comparison to shControl cells after stimulation with retinoic acid was overlapped with the common ZRF1/RING1B/H2Aub target genes (see also Supplementary Fig. 9). **b**, Functional enrichment analysis of the 104 common target genes downregulated in shZRF1 cells. **c**, ChIP experiments were performed with ZRF1 antibodies and chromatin obtained from NT2 induced with retinoic acid (*THRA*, *FGF9*, *RARB* and *RARA*: 1 h retinoic acid; *PER1* and *USP20*: 3 h retinoic acid). The occupancy at promoters of the aforementioned genes was tested by quantitative PCR. Data are represented as mean ± s.e.m. ($n = 3$). **d**, The mRNA levels of the genes indicated were measured in NT2 shZRF1 and shControl cell lines after supplementing with retinoic acid for the respective times (*THRA*, *FGF9*, *PER1* and *USP20*: 3 h retinoic acid; *RARA* and *RARB*: 2 h retinoic acid). Data are represented as mean ± s.e.m. ($n = 3$). **e**, shControl, shZRF1 and shRING1B NT2 cells were induced for 1 h with $10^{-8}$ M of retinoic acid. RNA levels of the *HOXA1* and *HOXA2* mRNA were measured in relation to mRNA levels of the ribosomal gene *PUM1* ($n = 3$). **f**–**h**, shControl NT2 cells or shZRF1 knockdown cells were kept under the same conditions as in **e**, and chromatin was used in ChIP experiments with RING1B and ZRF1 antibodies. Data are represented as mean ± s.e.m. ($n = 3$). **i**, Mouse liver chromatin was incubated with ZRF1 and USP21 (10 or 20 ng) as indicated. The H2Aub levels were quantified after detection with specific antibodies.

Discussion). However, future research will have to reveal the dynamics of PRC1-catalysed ubiquitination.

## METHODS SUMMARY

Experiments were performed using human cell lines (NT2, 293T and U937) and affinity-purified or commercially available antibodies. The knockdown cells used were established by retroviral infection. ChIP experiments, mutagenesis of histone H2A, genome-wide studies and protein purification procedures are explained in Methods.

**Full Methods** and any associated references are available in the online version of the paper at www.nature.com/nature.

**Received 12 June 2009; accepted 12 October 2010.**


1. Strahl, B. D. & Allis, C. D. The language of covalent histone modifications. *Nature* **403,** 41–45 (2000).
2. Li, B., Carey, M. & Workman, J. L. The role of chromatin during transcription. *Cell* **128,** 707–719 (2007).
3. Kouzarides, T. Chromatin modifications and their function. *Cell* **128,** 693–705 (2007).
4. Goldknopf, I. L. *et al.* Isolation and characterization of protein A24, a "histone-like" non-histone chromosomal protein. *J. Biol. Chem.* **250,** 7182–7187 (1975).
5. Zhu, B. *et al.* Monoubiquitination of human histone H2B: the factors involved and their roles in *HOX* gene regulation. *Mol. Cell* **20,** 601–611 (2005).
6. Nickel, B. E., Allis, C. D. & Davie, J. R. Ubiquitinated histone H2B is preferentially located in transcriptionally active chromatin. *Biochemistry* **28,** 958–963 (1989).
7. Wang, H. *et al.* Role of histone H2A ubiquitination in Polycomb silencing. *Nature* **431,** 873–878 (2004).
8. Kuzmichev, A., Nishioka, K., Erdjument-Bromage, H., Tempst, P. & Reinberg, D. Histone methyltransferase activity associated with a human multiprotein complex containing the Enhancer of Zeste protein. *Genes Dev.* **16,** 2893–2905 (2002).
9. Zhou, W. *et al.* Histone H2A monoubiquitination represses transcription by inhibiting RNA polymerase II transcriptional elongation. *Mol. Cell* **29,** 69–80 (2008).
10. Pan, X. *et al.* A DNA integrity network in the yeast *Saccharomyces cerevisiae*. *Cell* **124,** 1069–1081 (2006).
11. Greiner, J. *et al.* Characterization of several leukemia-associated antigens inducing humoral immune responses in acute and chronic myeloid leukemia. *Int. J. Cancer* **106,** 224–231 (2003).
12. Resto, V. A. *et al.* A putative oncogenic role for MPP11 in head and neck squamous cell cancer. *Cancer Res.* **60,** 5529–5535 (2000).
13. Inoue, T., Shoji, W. & Obinata, M. MIDA1, an Id-associating protein, has two distinct DNA binding activities that are converted by the association with Id1: a novel function of Id protein. *Biochem. Biophys. Res. Commun.* **266,** 147–151 (1999).
14. Hicke, L., Schubert, H. L. & Hill, C. P. Ubiquitin-binding domains. *Nature Rev. Mol. Cell Biol.* **6,** 610–621 (2005).
15. Bracken, A. P., Dietrich, N., Pasini, D., Hansen, K. H. & Helin, K. Genome-wide mapping of Polycomb target genes unravels their roles in cell fate transitions. *Genes Dev.* **20,** 1123–1136 (2006).
16. Lee, M. G. *et al.* Demethylation of H3K27 regulates polycomb recruitment and H2A ubiquitination. *Science* **318,** 447–450 (2007).
17. Saito, S. *et al.* Haptoglobin-β chain defined by monoclonal antibody RM2 as a novel serum marker for prostate cancer. *Int. J. Cancer* **123,** 633–640 (2008).
18. Andrews, P. W. Retinoic acid induces neuronal differentiation of a cloned human embryonal carcinoma cell line *in vitro*. *Dev. Biol.* **103,** 285–293 (1984).
19. Andrews, P. W. *et al.* Pluripotent embryonal carcinoma clones derived from the human teratocarcinoma cell line Tera-2. Differentiation *in vivo* and *in vitro*. *Lab. Invest.* **50,** 147–162 (1984).
20. Boyer, L. A. *et al.* Polycomb complexes repress developmental regulators in murine embryonic stem cells. *Nature* **441,** 349–353 (2006).
21. Kallin, E. M. *et al.* Genome-wide uH2A localization analysis highlights Bmi1-dependent deposition of the mark at repressed genes. *PLoS Genet.* **5,** e1000506 (2009).
22. O'Geen, H. *et al.* Genome-wide analysis of KAP1 binding suggests autoregulation of KRAB-ZNFs. *PLoS Genet.* **3,** e89 (2007).
23. Pasini, D., Bracken, A. P., Hansen, J. B., Capillo, M. & Helin, K. The polycomb group protein Suz12 is required for embryonic stem cell differentiation. *Mol. Cell. Biol.* **27,** 3769–3779 (2007).
24. Villa, R. *et al.* Role of the polycomb repressive complex 2 in acute promyelocytic leukemia. *Cancer Cell* **11,** 513–525 (2007).
25. Nakagawa, T. *et al.* Deubiquitylation of histone H2A activates transcriptional initiation via trans-histone cross-talk with H3K4 di- and trimethylation. *Genes Dev.* **22,** 37–49 (2008).
26. Levinger, L. & Varshavsky, A. Selective arrangement of ubiquitinated and D1 protein-containing nucleosomes within the *Drosophila* genome. *Cell* **28,** 375–385 (1982).
27. Lagarou, A. *et al.* dKDM2 couples histone H2A ubiquitylation to histone H3 demethylation during Polycomb group silencing. *Genes Dev.* **22,** 2799–2810 (2008).
28. Doil, C. *et al.* RNF168 binds and amplifies ubiquitin conjugates on damaged chromosomes to allow accumulation of repair proteins. *Cell* **136,** 435–446 (2009).


**Supplementary Information** is linked to the online version of the paper at www.nature.com/nature.

**Acknowledgements** We are indebted to S. Jentsch, S. Berger, K. Helin, J. Hasskarl, R. Shiekattar, T. Zimmermann and V. Raker for antibodies and plasmids and for discussions; and to the CRG Microarray facility and Light Microscopy Facility. This work was supported by the Spanish "Ministerio de Educación y Ciencia" (BFU2007-63059), the Association for International Cancer Research (10-0177), by the AGAUR and Consolider to L.D.C., and by FOR967 to S.R.; H.R. was supported by a FEBS fellowship; J.R. by a fellowship from Fundação para a Ciência e Tecnologia; L.R.-V. by a Juan de la Cierva Fellowship; S.D. by a PFIS fellowship.

**Author Contributions** H.R. cloned, purified proteins and performed biochemical studies. H.R., L.R.-V., J.D.R. and S.D. performed ChIP analysis. G.G. and N.L.-B. performed genome-wide analysis. T.N. and T.I. performed *in vitro* transcription and deubiquitination experiments. S.R. provided essential tools. H.R. and L.D.C. designed the experiments, supervised the project and wrote the manuscript. All authors commented on the manuscript.

**Author Information** Reprints and permissions information is available at www.nature.com/reprints. The authors declare no competing financial interests. Readers are welcome to comment on the online version of this article at www.nature.com/nature. Correspondence and requests for materials should be addressed to L.D.C. (luciano.dicroce@crg.es).

## METHODS

**Plasmids, antibodies and cell lines.** Antibodies against ZRF1 and RING1B were either previously described[29], or raised in rabbits against full-length protein and affinity purified. To that end, GST fusion proteins of both proteins were cross-linked to glutathione beads and packed into polystyrol mini-columns (Pierce). Antisera were repeatedly run over the columns, washed and finally eluted in Tris buffer pH 2.5. The affinity-purified antibody was finally set to pH 8.0. For Fig. 1d the ZRF1 serum against full-length protein was used to visualize the recombinant protein deletion mutants. In all other experiments the antibody purified with GST–ZRF1ΔSANT (a ZRF1 protein lacking the C-terminal SANT domains) was used. Antibodies against H2Aub, IgM conjugating antibody and H3K4 trimethyl were obtained from Upstate antibodies. Antibodies against histone H2A and the histone modification H3K4 trimethyl were purchased from Abcam. Antibodies against the His and Flag epitopes were purchased from Qiagen and SIGMA, respectively. Antibodies against EED and SUZ12 were a gift from K. Helin. Plasmids for the ectopic expression of Flag-tagged ID proteins were a gift from J. Hasskarl. For tagging proteins the pet28 (His tag, Novagen), pCMV2 (Flag, Invitrogen) and pGex (GST, Invitrogen) vector series were used. The ZRF1 specific sequences GTTATCTGATCCAGTGAAA and GATCAAAGCAGCTCATAAA were used to synthesize oligonucleotides and cloned into pRetroSuper[30]. In the case of RING1B the specific sequences AGAACACCATGACTACAAA and TTCTAAAGCTAACCTCACA were cloned into the same vector. Mutagenesis of histone H2A was performed using the Quikchange mutagenesis kit (Stratagene) on a pCMV2b histone H2A plasmid. Information on the cloning and sequences are available upon request. The embryonic carcinoma cell line NTERA2 (NT2/D1) and HEK 293T cells were cultured in DMEM medium supplemented with 10% fetal bovine serum at 37 °C and 5% $CO_2$. NT2 cells were treated with retinoic acid to induce differentiation at the given concentrations for the mentioned time intervals. U937 cells were cultured in RPMI medium at 37 °C and 5% $CO_2$.

**Purification of recombinant proteins.** Proteins were purified as suggested by Qiagen (His-tagged proteins) and Amersham (GST-tagged proteins) after inducing BL21 bacterial strains transformed with the respective plasmids at an optical density of 0.5 with 0.2 mM of isopropyl-β-D-thiogalactoside either for 4 h at 37 °C or at 20 °C for 14 h.

**Purification of ubiquitin-binding proteins.** HEK 293T cells were transfected with pCMV2b-histone H2A or the corresponding empty vector (Control) and after 48 h mononucleosomes were purified by means of the Flag epitope as stated in Supplementary Fig. 1A, C. After harvesting by centrifugation, cells were resuspended in buffer A (10 mM HEPES pH 7.9, 1.5 mM $MgCl_2$, 10 mM KCl and 0.5 mM dithiothreitol (DTT), phenylmethylsulphonyl fluoride (PMSF)) and homogenized by 10 strokes in a Dounce homogenizer with a B-type pestle. After centrifugation, nuclei were resuspended in lysis buffer (137 mM NaCl, 2.7 mM KCl, 10 mM $NaH_2PO_4$, 2 mM $KH_2PO_4$, 0.1% Triton X-100, 0.5 mM DTT, PMSF) and sonified using a Diagenode Bioruptor to obtain mononucleosomes (4 °C, 4 cycles of 15 min, 'H' setting). Protein extracts were then subjected to centrifugation (16,100*g*, 4 °C, 30 min) to remove debris and incubated with M2-Flag Agarose beads. The bound material or the control beads (M2-beads incubated with protein extracts from control transfections) were poured in polystyrol mini-columns (Flag–H2A column and Control column), washed intensively with lysis buffer and then used subsequently in an affinity purification. To this end, a nuclear protein extract devoid of histone proteins was prepared from 293T cells as previously described[31]. In brief, nuclei were extracted by resuspension of cells in buffer A (10 mM HEPES pH 7.9, 1.5 mM $MgCl_2$, 10 mM KCl and 0.5 mM DTT, PMSF) and homogenized by 10 strokes in a Dounce homogenizer with a B-type pestle. The crude nuclei were resuspended in buffer C (20 mM HEPES pH 7.9, 25% (v/v) glycerol, 1.5 mM $MgCl_2$, 420 mM NaCl, 0.2 mM EDTA, 0.5 mM DTT and PMSF) and homogenized in a Dounce homogenizer (10 strokes, B-type pestle). The resulting protein suspension was stirred by a magnetic stirring bar for 30 min at 4 °C and then centrifuged at 25,000*g* in an SS34 rotor for 3 h. The resulting supernatant was dialysed against lysis buffer, and run in a loop over two polystyrol mini-columns (Flag–H2A column and Control column; see above). After intensive washing with lysis buffer the columns were incubated with a solution of lysis buffer with recombinant His-tagged ubiquitin previously purified by Ni-NTA Agarose (Qiagen) and gel filtration on a Superose 12 column. After eluting the ubiquitin-binding proteins, the columns were washed again in lysis buffer and mononucleosomes were subsequently eluted by a solution of Flag peptide in lysis buffer. Both eluates were subjected to electrophoresis, stained with colloidal coomassie, and possible interactors were subjected to MALDI-Fingerprint analysis.

**Transfection and retroviral infection.** Transfection of HEK 293T cells was usually performed by the calcium phosphate co-precipitation method as described[24]. pRS-based retrovirus was produced by transfecting the GP2-293 packaging cell line (Clontech). The collected retrovirus was subsequently used to transduce NT2 or 293T cell lines by spinoculation at 900*g* for 90 min at 32 °C in the presence of protamine sulphate. After incubating overnight at 37 °C the protocol was repeated for two consecutive days.

**M2-Flag affinity chromatography.** Purification of Flag-tagged proteins from 293T cells was essentially done as described earlier. All experiments with Flag-tagged histone H2A were performed in polystyrene mini-columns (Pierce) with subsequent elution using the Flag peptide (Sigma) at a concentration of 100 μg $ml^{-1}$ in PBS.

**ZRF1–H2Aub interaction experiments.** Nuclear protein extracts were prepared as described earlier to obtain mononucleosomes. The protein extract was then incubated with or without recombinant His–ZRF1 (lanes ZRF1 and Control in Fig. 1c) for 4 h at 4 °C. Ni-NTA Agarose was added and after 2 h of incubation at 4 °C the beads were washed intensively with lysis buffer. The precipitated material was then subjected to western blotting.

**Nucleosome–RING1B complexes and *in vitro* assays.** Mononucleosomes were purified as described earlier, but washed with lysis buffer containing 450 mM NaCL and maintained at the Flag-M2 Agarose beads. The bound nucleosomes and empty M2 beads were subsequently incubated with bacterial extracts in lysis buffer containing recombinant His–RING1B. After 2 h of incubation at 4 °C the beads were washed in the same buffer intensively (see Supplementary Fig. 2C). The RING1B–nucleosome complexes were then incubated with equal or equimolar amounts of either GST or GST–ubiquitin (Fig. 2b) or ZRF1 (Fig. 2g) in lysis buffer. After 2 h of incubation at 4 °C the beads were packed into polystyrole columns, washed and eluted with Flag peptide at 100 μg $ml^{-1}$. The eluate was finally subjected to immunoblotting.

**ChIP.** ChIP experiments were essentially performed as described[24]. For all experiments affinity-purified antibodies were used as described earlier. The immunoprecipitated DNA was quantified by real-time quantitative PCR (Roche Lightcycler). The primers for verifying the occupancy of the immunoprecipitated protein at chromatin are available upon request.

**Genome-wide mapping of ZRF1 target genes (ChIP-on-chip).** Chromatin from NT2 cells before (0 h) and after induction with retinoic acid ($10^{-8}$ M) for 1 h or 3 h was subjected to ChIP experiments with ZRF1 and control antibodies. For each time-point of the ChIP experiments triplicates were carried out. The obtained material was amplified with the WGA kit (Sigma) and linear amplification of the material was tested in qPCR reactions with known ZRF1 targets. Labelling and hybridization to Agilent Human Promoter Arrays were carried out following the supplier's instructions. Analogously, chromatin from unstimulated NT2 cells was subjected to ChIP experiments with RING1B, H2Aub and the respective conjugating antibody. The obtained material was processed as described earlier.

**Microarray analysis.** Microarray analysis was performed after extracting a triplicate of three different biological samples of RNA from NT2 cells lines (shZRF1 and shControl) either from non-induced cells or cells induced with retinoic acid ($10^{-8}$ M, 3 h). RNA was amplified, labelled and subsequently hybridized to a Human Genome Oligo Microarray (Agilent). Raw data were analysed using the Limma package.

**Data analysis and statistics.** Absolute foreground and background readings from channels were used as input to the chipper program. Default parameters were used as defined previously[32]. Chipper calculates $q$ values (corrected $P$ values), thus accounting for multiple testing corrections per probe. Probes with $q$ values $<0.05$ were accepted as significant. Probes, which are significantly bound by ZRF1, were compared to those significantly bound by IgG to subtract IgG targets. ZRF1 targets were mapped to genes according to the information provided by Agilent. To study significant overlapping between genes bound by ZRF1 and genes bound by SUZ12, RING1B, H2Aub or the H3K27me3 mark, respectively, the enrichment analysis (EA) method was applied. The statistical significance ($P$ value) was calculated using the binomial distribution. Significance levels were corrected for multiple comparisons with the Benjamini and Hochbert method. Functional enrichment analysis was performed with the DAVID software[33].

**RNA preparation and analysis by quantitative PCR.** RNA was extracted with the RNeasy mini kit (Qiagen) and transcribed to cDNA by reverse transcription using the AMV kit (Roche). The expression of the respective genes was assayed by quantitative real-time PCR (Roche Lightcycler). As a reference, the expression of GAPDH or PUM1 was measured for each experiment. The sequences of the primers are available upon request.

**GST pull-down.** Purified GST–proteins were bound in equimolar amounts to glutathione beads (Amersham) in binding buffer (20 mM Tris pH 8.0, 150 mM NaCl, 0.5% NP-40). Loaded beads were washed in the same buffer and used for incubation with recombinant proteins for 2 h at 4 °C. For the competition assay (Fig. 2e) with recombinant ZRF1 and RING1B, the amounts of RING1B were kept constant and the amounts of ZRF1 were increased with every consecutive pull-down until finally reaching equimolar conditions. For preassembling RING1B–ubiquitin complexes (Fig. 2f), GST and GST–ubiquitin were bound to beads,

washed and incubated with RING1B at 4 °C for 2 h. Loaded beads were then incubated with a roughly tenfold higher amount of ZRF1-UBD together with an excess of BSA—where stated—for 90 min at 4 °C. Finally, beads were washed intensively in binding buffer, denatured in SDS buffer, and subjected to electrophoresis and subsequent western blotting analysis.

**Gel-filtration analysis.** Gel-filtration was performed on an AEKTA-Explorer system (Amersham) using Superose12 or Superose6 columns (Amersham). After calibrating the column with specific proteins, a solution of recombinant protein in PBS was injected and the UV-elution profile was detected. To verify each volume of elution the fractions were subjected to western blotting by probing with specific antibodies.

**Chromatin association assays.** Cells were crosslinked with a solution of 1% formaldehyde in PBS for 10 min at 24 °C. Nuclei were prepared by resuspending the cell pellets in buffer A (100 mM Tris pH 7.5, 5 mM $MgCl_2$, 60 mM KCl, 0.5 mM DTT, 125 mM NaCl, 300 mM sucrose, 1% NP-40). After lysis on ice the nuclei were pelleted and resuspended in buffer B (100 mM Tris pH 7.5, 1 mM $CaCl_2$, 60 mM KCl, 0.5 mM DTT, 125 mM NaCl, 300 mM sucrose) and supplemented with 10 U of MNase I for 20 min at 37 °C. The reaction was stopped by adding EDTA. The chromatin was pelleted and resuspended in buffer C (1% SDS, 10 mM EDTA, 50 mM Tris pH 8.0) overnight at 4 °C. After centrifugation (16,100*g*, 2 min) the supernatant was used for western blotting.

***In vitro* deubiquitination assays.** Deubiquitination experiments were essentially performed as previously described[25]. In short, mouse liver chromatin was incubated with no or increasing amounts of recombinant ZRF1. Subsequently USP21 was added and reactions were incubated at 37 °C for 18 min.


29. Otto, H. *et al.* The chaperones MPP11 and Hsp70L1 form the mammalian ribosome-associated complex. *Proc. Natl Acad. Sci. USA* **102,** 10064–10069 (2005).
30. Brummelkamp, T. R., Nijman, S. M., Dirac, A. M. & Bernards, R. Loss of the cylindromatosis tumour suppressor inhibits apoptosis by activating NF-κB. *Nature* **424,** 797–801 (2003).
31. Dignani, J. D., Lebovitz, R. M. & Roeder, R. G. Accurate transcription initiation by RNA polymerase II in a soluble extract from isolated mammalian nuclei. *Nucleic Acids Res.* **11,** 1475–1489 (1983).
32. Gibbons, F. D., Proft, M., Struhl, K. & Roth, F. P. Chipper: discovering transcription-factor targets from chromatin immunoprecipitation microarrays using variance stabilization. *Genome Biol.* **6,** R96 (2005).
33. Huang, D. W., Sherman, B. T. & Lempicki, R. A. Systematic and integrative analysis of large gene lists using DAVID bioinformatics resources. *Nature Protocols* **4,** 44–57 (2009).

OPEN ACCESS Freely available online PLoS GENETICS

# The Meiotic Recombination Checkpoint Suppresses NHK-1 Kinase to Prevent Reorganisation of the Oocyte Nucleus in *Drosophila*

**Oscar M. Lancaster[1¤], Manuel Breuer[1], C. Fiona Cullen[1], Takashi Ito[2], Hiroyuki Ohkura[1]***

**1** The Wellcome Trust Centre for Cell Biology, School of Biological Sciences, University of Edinburgh, Edinburgh, United Kingdom, **2** Department of Biochemistry, Nagasaki University School of Medicine, Nagasaki, Japan

## Abstract

The meiotic recombination checkpoint is a signalling pathway that blocks meiotic progression when the repair of DNA breaks formed during recombination is delayed. In comparison to the signalling pathway itself, however, the molecular targets of the checkpoint that control meiotic progression are not well understood in metazoans. In *Drosophila*, activation of the meiotic checkpoint is known to prevent formation of the karyosome, a meiosis-specific organisation of chromosomes, but the molecular pathway by which this occurs remains to be identified. Here we show that the conserved kinase NHK-1 (*Drosophila* Vrk-1) is a crucial meiotic regulator controlled by the meiotic checkpoint. An *nhk-1* mutation, whilst resulting in karyosome defects, does so independent of meiotic checkpoint activation. Rather, we find unrepaired DNA breaks formed during recombination suppress NHK-1 activity (inferred from the phosphorylation level of one of its substrates) through the meiotic checkpoint. Additionally DNA breaks induced by X-rays in cultured cells also suppress NHK-1 kinase activity. Unrepaired DNA breaks in oocytes also delay other NHK-1 dependent nuclear events, such as synaptonemal complex disassembly and condensin loading onto chromosomes. Therefore we propose that NHK-1 is a crucial regulator of meiosis and that the meiotic checkpoint suppresses NHK-1 activity to prevent oocyte nuclear reorganisation until DNA breaks are repaired.

**Citation:** Lancaster OM, Breuer M, Cullen CF, Ito T, Ohkura H (2010) The Meiotic Recombination Checkpoint Suppresses NHK-1 Kinase to Prevent Reorganisation of the Oocyte Nucleus in *Drosophila*. PLoS Genet 6(10): e1001179. doi:10.1371/journal.pgen.1001179

**Editor:** R. Scott Hawley, Stowers Institute for Medical Research, United States of America

**Received** November 25, 2009; **Accepted** September 24, 2010; **Published** October 28, 2010



**Funding:** OML and HO received a BBSRC Special Studentship and a Wellcome Trust Senior Research Fellowship, respectively. This work is supported by The Wellcome Trust (www.wellcome.ac.uk). The funders had no role in study design, data collection and analysis, decision to publish, or preparation of the manuscript.

**Competing Interests:** The authors have declared that no competing interests exist.

* E-mail: h.ohkura@ed.ac.uk

¤ Current address: Medical Research Council Laboratory for Molecular Cell Biology, Division of Life Sciences, University College London, London, United Kingdom

## Introduction

Meiosis is a specialised form of cell division that differs from mitosis in many respects, particularly during the exchange of genetic information between homologous chromosomes in recombination. In early meiotic prophase, DNA double-strand breaks (DSBs) are introduced into meiotic chromosomes by the conserved enzyme Spo11 to initiate recombination [1–4]. An elaborate structure, the synaptonemal complex, then forms between homologous chromosomes stabilising their pairing and recombination [5]. Once recombination is complete and DSBs have been repaired, the synaptonemal complex is disassembled. As these events are meiosis-specific, molecular mechanisms of meiotic prophase progression need to be established beyond our understanding of mitotic cell cycle control.

Eukaryotes have a surveillance-signalling system, the so-called meiotic recombination checkpoint (hereafter referred to as the meiotic checkpoint), which prevents meiotic progression until DSBs generated during recombination are repaired [6–8]. Many advances have been made recently in determining the mechanisms involved in the detection of and signalling downstream from DSBs [9]. In contrast, little is known about how the checkpoint signal blocks meiotic progression, except in yeast. In yeast, the Cdc28 (Cdk1)-Cyclin complex is suppressed in various ways by the meiotic checkpoint to delay or block meiotic division [10–12].

In *Drosophila*, the meiotic checkpoint was first revealed by the study of a class of mutants collectively called *spindle* (*spn*) mutants. These *spn* mutants were originally identified based on their abnormal dorsal-ventral oocyte polarity [13–16]. They also share abnormalities in a meiosis-specific organisation of chromosomes called the karyosome [14,17,16].

The meiotic checkpoint pathway is activated in *spn* mutants by persistent DSBs caused either by defects in DNA repair during recombination [18,19] or in processing of repeat-associated siRNA that suppress germline retrotransposition [20–22]. Signalling downstream of DSBs in the meiotic checkpoint requires the successive activation of two conserved kinases, Mei-41 (an ATM/ATR homologue) and Mnk/Chk2 [17,23]. Their activation blocks both oocyte polarisation and karyosome formation. Vasa was proposed to act downstream of the meiotic checkpoint to mediate both oocyte polarisation and karyosome formation [17,23], but a more recent study suggests that Vasa acts upstream of the checkpoint through involvement in processing of repeat-associated siRNA [24]. Gurken has been shown to be a downstream effector required for oocyte polarisation which is inhibited by the meiotic checkpoint [25,16], but an effector required for karyosome formation has not been identified.

## Author Summary

Meiosis is a specialised form of cell division that produces haploid gametes from diploid cells. Failures or errors in meiosis can lead to infertility, miscarriages, or birth defects. In meiosis, chromosomes first swap genetic information during recombination and then undergo two rounds of segregation. Temporal separation of these distinct meiotic events is essential for successful meiosis. To ensure this correct temporal order, the meiotic recombination checkpoint blocks meiotic progression when recombination is not completed. Adding to our understanding of this process, we here report that the conserved *Drosophila* protein kinase NHK-1 is a crucial regulator of meiosis that is controlled by the meiotic recombination checkpoint. The meiotic recombination checkpoint suppresses the activity of NHK-1 to block transitional remodelling of meiotic chromosomes in the oocyte nucleus until recombination is completed.


The karyosome is a compact cluster of meiotic chromosomes formed within the *Drosophila* oocyte nucleus [26] and similar structures are also found in human oocytes [27]. In addition to the successful completion of recombination, recent studies by us and others have shown that nucleosomal histone kinase-1 (NHK-1) is essential for karyosome formation [28,29]. NHK-1 is a Histone 2A kinase conserved from nematodes to humans (Vrk-1 in *C. elegans*, and Vrk1-3 in mammals) [30]. We showed that NHK-1 also phosphorylates Barrier-to-Autointegration Factor (BAF) to release meiotic chromosomes from the oocyte nuclear envelope during karyosome formation [31]. However nothing is known about how NHK-1 activity itself might be controlled during meiosis.

In this report, we have investigated the functional relationship between NHK-1 and the meiotic checkpoint. We found that the meiotic checkpoint suppresses NHK-1 activity to prevent reorganisation of the oocyte nucleus, including karyosome formation, synaptonemal complex disassembly and condensin loading, until DNA breaks are repaired. Therefore, we propose that NHK-1 is a critical meiotic regulator controlled by the meiotic checkpoint.

## Results/Discussion

### The meiotic checkpoint pathway is not activated in an *nhk-1* mutant

In the wild-type oocyte nucleus, meiotic chromosomes are clustered together to form a spherical body called the karyosome [26] (Figure 1C). Female sterile *nhk-1* mutations show an abnormal morphology of the karyosome, which is less compact and often attached to the nuclear envelope [28,29,31] (Figure 1B and Figure S1). A similar karyosome abnormality is also observed in the *spn* class of mutants, which were originally identified based on their abnormal oocyte polarity [13,14,16,17] (Figure 1A and Figure S1). Most *spn* mutants contain persistent DNA double stranded breaks (DSBs) in meiotic chromosomes and activate the meiotic checkpoint pathway [18–22]. Both the karyosome and polarity defects in these *spn* mutants can be rescued by inactivation of the meiotic checkpoint [17,21,23] (Figure 1D).

A possible explanation for this similarity in the karyosome defects between *nhk-1* and *spn* mutants is that *nhk-1* mutations lead to an activation of the meiotic checkpoint pathway. To test this possibility, we assessed the activation of the meiotic checkpoint pathway in an *nhk-1* mutant by examining for the persistence of DSBs on meiotic chromosomes and the presence of oocyte/embryo polarity defects. The $nhk\text{-}1^{23\text{-}0437}$ mutant has been previously shown to have no delay in DSB repair or polarity defects [28]. However, as this allele contains a mis-sense mutation in a residue with unknown function in the kinase domain, the phenotype may be due to the specific nature of this allele. To exclude this possibility, we examined another female sterile allele, $nhk\text{-}1^{E24/Df}$, that expresses a reduced amount of wild-type NHK-1 protein and shows karyosome defects [29,31]. To assess oocyte polarity, we examined the dorsal appendages of eggs laid by females, whose formation depends on correct dorsal-ventral axis specification in the oocyte [32]. Dorsal appendages of eggs laid by the $nhk\text{-}1^{E24/Df}$ mutant did not show abnormalities, indicating that oocyte polarity was properly established. Furthermore, immunostaining using an antibody against the phosphorylated form of the *Drosophila* H2AX variant (γ-H2Av) which accumulates at DSB sites [33] showed no detectable DSB foci at late oogenesis stages, indicating DSBs were repaired in the $nhk\text{-}1^{E24/Df}$ mutant (Figure S2). These results indicated that, unlike *spn* mutants, the meiotic

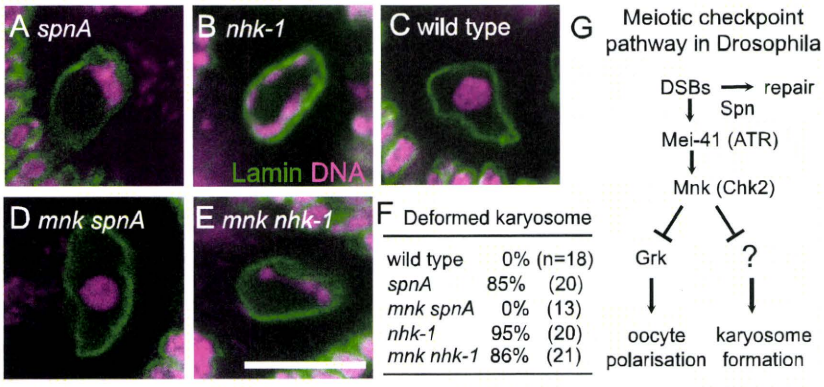


**Figure 1. Inactivation of the meiotic checkpoint did not suppress *nhk-1* karyosome defects.** The karyosome morphology in an oocyte from $spnA^{1}$ (A), $nhk\text{-}1^{E24/Df}$ (B), wild type (C), an $mnk^{p6}$ $spnA^{1}$ double mutant (D), and an $mnk^{p6}$ $nhk\text{-}1^{E24/Df}$ double mutant (E). Bar = 10 μm. (F) The frequency of deformed karyosomes in oocytes with various genotypes. Inactivation of the meiotic checkpoint by the $mnk^{p6}$ mutation rescued the karyosome defect in $spnA^{1}$ ($p<0.01$), but not in $nhk\text{-}1^{E24/Df}$ (G) The meiotic recombination checkpoint pathway in *Drosophila* oocytes (modified from 23).
doi:10.1371/journal.pgen.1001179.g001

checkpoint pathway is not activated in the *nhk-1*$^{E24/Df}$ mutant, despite the clear karyosome defect observed in this mutant.

## The karyosome defect in an *nhk-1* mutant does not require meiotic checkpoint activation

To further confirm that the karyosome defect in the *nhk-1*$^{E24/Df}$ mutant arises without meiotic checkpoint activation, we examined whether inactivating the checkpoint rescues the karyosome defect in the *nhk-1*$^{E24/Df}$ mutant. The meiotic checkpoint signalling pathway contains two kinases, Mei-41 and Mnk, which are homologues of ATM/ATR and Chk-2 respectively (Figure 1G). A mutation in either of these genes has been shown to rescue the karyosome defect caused by unrepaired DSBs in *spn* mutants (Figure 1D) [17,21,23], although *mei-41* mutations have been shown to be less proficient at rescuing the karyosome defect probably due to the presence of a second ATM/ATR homologue [21].

We constructed a double mutant between *nhk-1*$^{E24/Df}$ and *mnk* by successive genetic crosses, and immunostaining of oocytes was carried out to visualise the oocyte nucleus and the karyosome. This showed that inactivation of the meiotic checkpoint failed to rescue the karyosome defect in the *nhk-1*$^{E24/Df}$ mutant (Figure 1E and 1F). In an *mnk nhk-1* double mutant, 86% of oocytes showed deformed karyosome morphology, similar to the *nhk1* single mutant in which 95% of oocytes showed deformed karyosomes ($p>0.3$). In a control analysis done in parallel, no oocytes from an *mnk spnA* double mutant showed deformed karyosome morphology (Figure 1D and 1F), in comparison to 85% of oocytes from a *spnA* single mutant ($p<0.01$).

In conclusion, these results demonstrated that the karyosome defect in the *nhk-1*$^{E24/Df}$ mutant is not caused by activation of the meiotic checkpoint pathway.

## Unrepaired DSBs suppress NHK-1 kinase activity

The above results demonstrated that the *nhk-1*$^{E24/Df}$ mutation induces karyosome defects without activation of the meiotic checkpoint pathway. Therefore, this places NHK-1 function either downstream or in parallel to the meiotic checkpoint pathway. One way to distinguish between these two possibilities would be to examine the kinase activity of NHK-1 in oocytes under conditions activating the meiotic checkpoint pathway (ie. in *spn* mutants). It is known that NHK-1 directly phosphorylates Histone 2A (H2A) at threonine 119 (T119; 30), and this phosphorylation in the oocyte nucleus has been shown to depend on NHK-1 activity [28]. Therefore we decided to examine the level of H2A T119 phosphorylation in the oocyte nucleus as a readout of NHK-1 activity *in vivo* by immunostaining using a phospho-specific antibody (anti-dH2ApT119) [30].

Ovaries from *spn* mutants (*spnA*, *spnB*, *spnD* and *vasa*) were dissected and immunostained with the anti-dH2ApT119 antibody. As a control, we also examined wild type and the *nhk-1*$^{E24/Df}$ mutant in parallel. Compared to wild type, we found that the H2ApT119 signal was greatly reduced on meiotic chromosomes in oocytes from *spn* mutants, as well as in oocytes from the *nhk-1*$^{E24/Df}$ mutant (Figure 2A and Figure S3A).

To quantify the level of the H2ApT119 signal reproducibly and comparably between different oocytes, we measured the H2ApT119 signal in the oocyte nucleus relative to that in follicle cell nuclei, in which H2A T119 phosphorylation has been shown to be independent of NHK-1 activity [28]. H2ApT119 signals in *spn* mutants were significantly reduced ($p<0.01$; Figure 2B).

We considered the possibility that the reduction of H2ApT119 signal under meiotic checkpoint activation was simply due to abnormal karyosome morphology itself (and we were in fact measuring an artefact or a secondary consequence). First of all, this

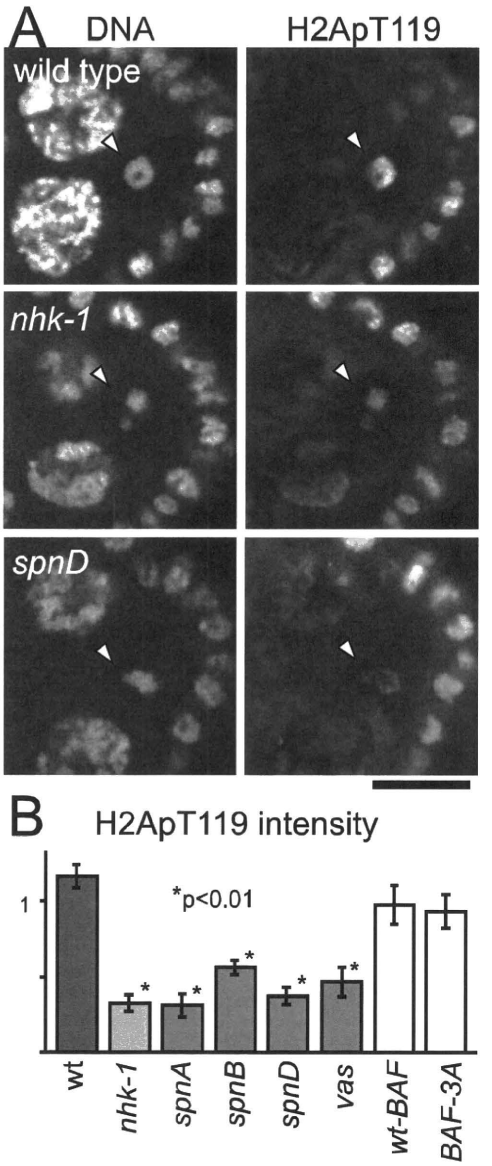


**Figure 2. Unrepaired DNA breaks suppress NHK-1 kinase activity.** (A) H2A T119 phosphorylation in wild type, *nhk-1*$^{E24/Df}$ and *spnD*$^{2}$. Ovaries at stage 5–7 were immunostained with anti-dH2ApT119 antibody and propidium iodide. Arrowheads indicate meiotic chromosomes in oocytes. Bar = 10 μm. (B) The H2ApT119 signal intensity on the chromosomes in oocytes was measured relative to that in follicle cells. The bars on the graph represent standard error of the mean (SEM). A minimum of eight oocytes from each genotype were quantified. NHK-1 activity measured by H2A T119 phosphorylation was significantly reduced in *nhk-1* and *spn* mutant oocytes ($p<0.01$; marked with asterisks). H2A T119 phosphorylation in oocytes expressing wild-type BAF and non-phosphorylatable BAF (BAF-3A) was comparable to that in wild type, indicating the karyosome abnormality itself is not the cause of low dH2ApT119 signals in *spn* mutants.
doi:10.1371/journal.pgen.1001179.g002

is unlikely because H2ApT119 signals were also reduced in karyosomes which retained relatively normal morphology in the *spn* mutants (Figure 2A and Figure S3A). To exclude this

possibility further, we took advantage of our previous study showing that expressing a non-phosphorylatable version of BAF (a substrate of NHK-1) disrupts the karyosome in these oocytes [31]. Under these conditions, although the karyosome was disrupted, the level of H2ApT119 signal in the oocyte nucleus was comparable to that in oocytes expressing wild-type BAF (that show normal karyosome morphology) or wild-type oocytes (Figure 2B and Figure S3B). Furthermore, to exclude the possibility that the apparent reduction in H2ApT119 was simply due to reduced chromosome condensation or DNA density, we re-quantified H2ApT119 signal intensity relative to DNA staining signal intensity in oocyte nuclei (Figure S3C). The H2ApT119 signal in the oocyte nucleus relative to that in follicle cell nuclei was divided by the DNA staining signal which had been measured using the same method. The result still showed a significant reduction in the H2ApT119 signal relative to DNA signal in *spn* mutant oocytes. The possibility that a simple reduction in H2A levels or its occupancy on DNA accounted for the decrease in H2Ap119 signal was further excluded by immunostaining using a phospho-independent antibody against H2A which did not show reduction in H2A signal in *spn* mutant oocytes (Figure S3D, S3E). These results confirm the genuine suppression of H2A T119 phosphorylation (which infers the suppression of NHK-1 activity) in these mutants.

Therefore we conclude that, judged by the phosphorylation level of one of its substrates, unrepaired DSBs in *spn* mutants suppress NHK-1 kinase activity in the oocyte nucleus.

## The meiotic checkpoint mediates suppression of NHK-1 activity

To confirm whether this suppression of NHK-1 activity by unrepaired DSBs is mediated by the meiotic checkpoint, we tested whether inactivation of the checkpoint (as shown in Figure 1) could abolish this suppression. Inactivation of the checkpoint was achieved by introduction of a mutation in *mnk*, which encodes the crucial checkpoint kinase Chk2. Examination of double mutants between *mnk* and *spnA* and between *mnk* and *spnD* showed that the H2ApT119 signal on meiotic chromosomes in *spn* mutants is restored by inactivation of the checkpoint (Figure 3 and Figure S4). This confirmed that the suppression of NHK-1 activity in the presence of DSBs is mediated by the meiotic checkpoint.

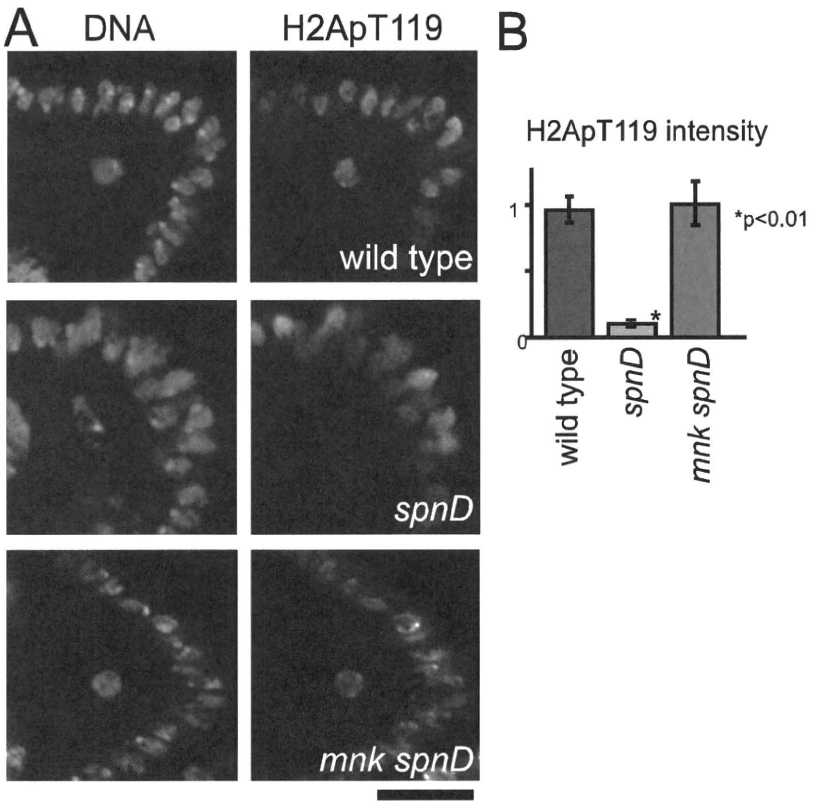


**Figure 3. The meiotic recombination checkpoint suppresses NHK-1 activity.** (A) H2A T119 phosphorylation in oocytes of wild type, *spnD*, and *mnk spnD*. Mnk (the Chk2 orthologue) is an essential kinase in the meiotic checkpoint. Ovaries at stage 5–7 were immunostained with anti-dH2ApT119 antibody and DAPI. (B) The H2ApT119 signal intensity on the chromosomes in oocytes was measured relative to that in follicle cells. The bars on the graph represent standard error of the mean (SEM). At least ten oocytes from each genotype were quantified. These samples were processed in parallel and compared only with each other, as exact values vary over time due to changes in factors including the conditions of the antibodies and fixative. NHK-1 activity measured by H2A T119 phosphorylation was significantly reduced in oocytes of a *spnD* mutant ($p<0.01$; marked with an asterisk), but not in those of an *mnk spnD* double mutant. Inactivation of the meiotic checkpoint rescued the suppression of NHK-1 activity in the presence of DSBs.
doi:10.1371/journal.pgen.1001179.g003

## DNA breaks suppress NHK-1 kinase activity in *Drosophila* cultured cells

Our cytological study showed that DSBs suppress the kinase activity of NHK-1, judged by phosphorylation of its substrate H2A at T119. We wished to confirm this suppression of NHK-1 activity by biochemical means. As biochemical measurements of oocyte-specific NHK-1 activity is challenging, we wondered whether similar suppression of NHK-1 may be observed when DSBs are induced in *Drosophila* cultured cells, without involvement of meiosis-specific factors.

To aid purification of NHK-1 from cultured cells (S2 cells), the NHK-1 gene was fused to GFP in frame and placed under the control of the metallothionein promotor. After transfection into S2 cells, a stable cell line inducibly expressing NHK-1-GFP was established. These cells were irradiated with X-rays at 1 Gy/min for 5 minutes. Immunostaining using a γ-H2Av antibody confirmed that this dose of X-rays efficiently induced DSBs without damaging the ability of cells to repair DSBs (data not shown). Fifteen minutes after X-ray irradiation, cells were collected and NHK-1-GFP was immunoprecipitated from cell extract using a GFP antibody in the presence of phosphatase inhibitors. The kinase activity of immunoprecipitated NHK-1-GFP was assayed *in vitro* by adding radioactive ATP without inclusion of exogenous substrates, as the NHK-1 substrate BAF is co-immunoprecipitated with NHK-1 [31].

Interestingly, we found that *in vitro* phosphorylation of co-immunoprecipitated BAF was greatly reduced in irradiated cells in comparison to non-irradiated cells processed in parallel (Figure 4A). This phosphorylation was dependent on NHK-1 kinase activity, as it was abolished by a mutation in NHK-1 [31] that eliminates its kinase activity but does not interfere with its binding to BAF (Figure 4A). Immunoblotting confirmed that comparable amounts of NHK-1 were immunoprecipitated from irradiated and non-irradiated samples (Figure 4A). When cells were collected 15 minutes after irradiation, their mitotic indexes were comparable (1.2% irradiated vs 1.4% non-irradiated), their nuclei still had unrepaired DSBs and nuclear localisation of NHK-1 was unaffected (Figure 4B). This indicates that the reduction in NHK-1 kinase activity in irradiated cells was not due to a reduction of mitotic cells or a change in NHK-1 localisation.

The suppression of NHK-1 kinase activity after X-ray irradiation was observed in three independent experiments. These biochemical results in S2 cells give further support to our observation in oocytes that NHK-1 kinase activity is suppressed in response to DSBs.

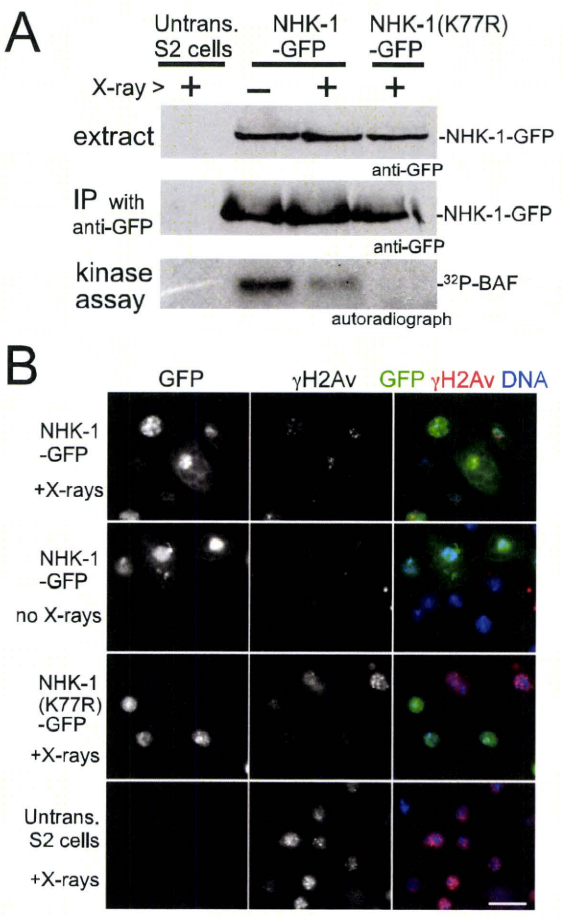


**Figure 4. DSBs suppress NHK-1 activity in S2 cells.** (A) Kinase activity of NHK-1-GFP was reduced after X-ray irradiation. S2 cells stably expressing NHK-1-GFP or NHK-1(K77R)-GFP, together with untransfected S2 cells, were irradiated with X-rays. Cells were collected 15 minutes later and NHK-1-GFP was immunoprecipitated from cell extracts by a GFP antibody. For the kinase assays, $^{32}$P-γATP was added and phosphorylation of co-immunoprecipitated BAF by NHK-1 was detected by autoradiograph. Cell extracts and immunoprecipitates used for kinase assays were immunoblotted with a GFP antibody. (B) DSBs were retained and the nuclear localisation of NHK-1-GFP was unaffected when cells were collected after X-ray treatment. DSBs and NHK-1-GFP were detected by immunostaining using antibodies against γH2Av and GFP, respectively. Bar = 10 μm.
doi:10.1371/journal.pgen.1001179.g004

## Activation of the meiotic checkpoint delays other NHK-1 dependent events

In addition to karyosome formation, NHK-1 has been shown to be required for the disassembly of the synaptonemal complex and loading of the condensin complex onto chromosomes during meiosis [28]. Our results showed that the meiotic checkpoint suppresses NHK-1 activity when DSBs are not repaired. From these observations, a prediction is that these other NHK-1 dependent events would also be blocked or delayed when the meiotic checkpoint pathway is activated. Indeed, a previous report showed that disassembly of the synaptonemal complex is delayed in a *spnA* mutant [18].

To test how universal this is, we examined the disassembly of the synaptonemal complex during oogenesis in various *spn* mutants. Immunostaining using an antibody against the synaptonemal complex protein C(3)G [34] showed that synaptonemal complex disassembly was significantly delayed in *spn* mutants. In wild-type oocytes, synaptonemal complex disassembly was completed by oogenesis stage 6. However, the characteristic filamentous structure of the synaptonemal complex or its remnants were still detected by the C(3)G antibody on meiotic chromosomes even at stage 6 or later in most oocytes of *spn* mutants (*spnA*, *spnB*, *spnD*; Figure 5A and Figure 4B). This delay in synaptonemal complex disassembly in *spn* mutants, but not in the *nhk-1*$^{Z3\text{-}0437/Df}$ mutant, was reversed by inactivation of the meiotic checkpoint using an *mnk* mutation (Figure S5).

Next we examined condensin loading onto meiotic chromosomes in wild type and *spn* mutants by immunostaining. In wild-type oocytes, the conserved condensin subunit CAP-D2 [35] is fully recruited onto meiotic chromosomes by stage 6 of oogenesis. In *spn* mutants, the protein had not fully accumulated onto meiotic

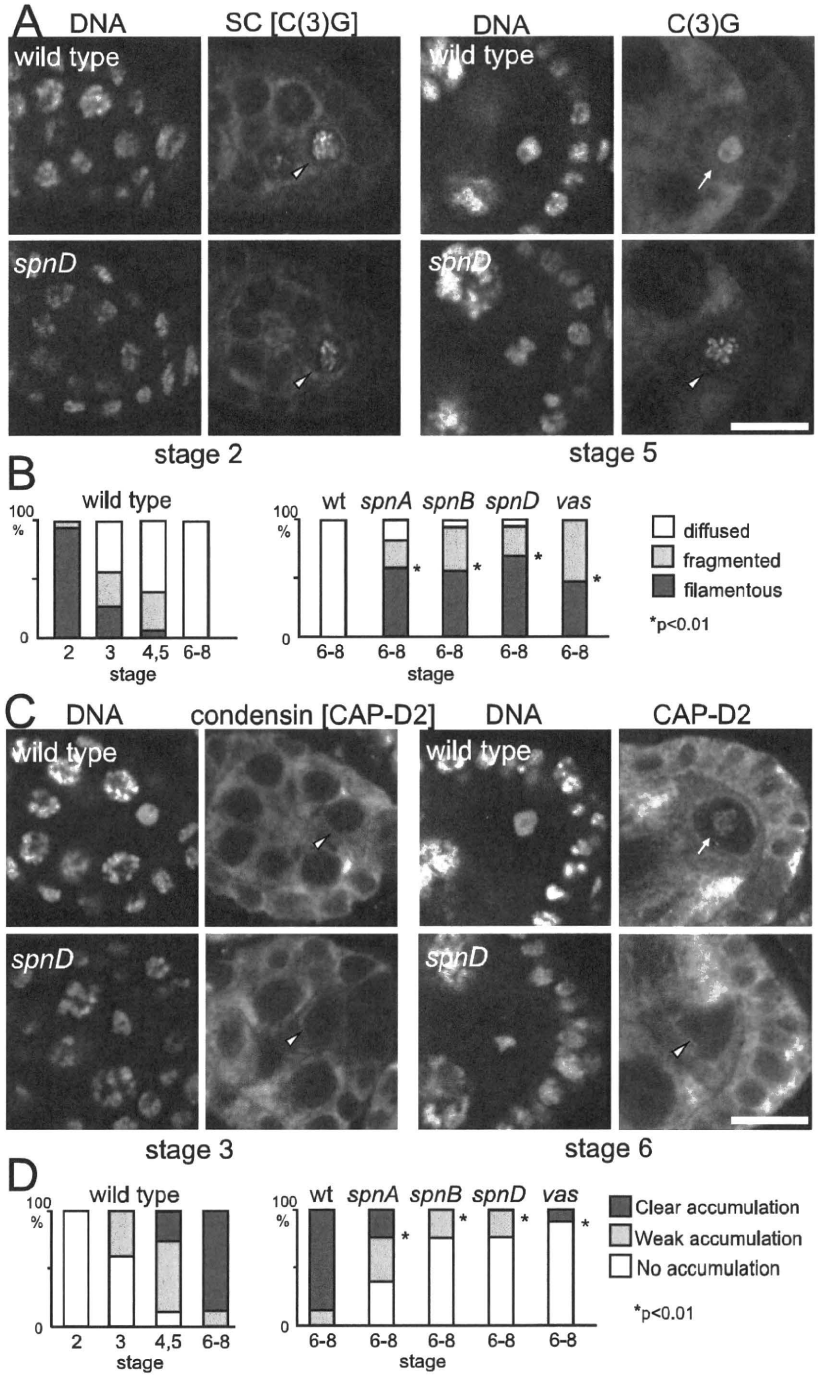


**Figure 5. Disassembly of the synaptonemal complex and loading of the condensin complex is delayed by meiotic checkpoint activation.** (A) Synaptonemal complex in wild-type and *spn* mutant oocytes. Ovaries were immunostained for the tranverse filament protein C(3)G and DNA. Bar = 10 μm. (B) The C(3)G staining pattern was classified as filamentous (arrowheads in A), fragmented or diffused (arrow in A). *spn* mutants significantly delayed disassembly of the synaptonemal complex ($p<0.01$; marked with asterisks). A minimum of thirteen oocytes were counted. (C) Condensin in wild-type and *spn* mutant oocytes. Ovaries were immunostained for the condensin subunit CAP-D2 and DNA. Bar = 10 μm. (D) Chromosome accumulation of CAP-D2 staining was classified into clear (arrow in C), weak or absent (arrowheads in C). *spn* mutants significantly delayed condensin loading ($p<0.01$; marked with asterisks). A minimum of nine oocytes were counted.
doi:10.1371/journal.pgen.1001179.g005

chromosomes in most oocytes even at stage 6 or later (Figure 5C and 5D), indicating that the condensin complex was not fully loaded onto meiotic chromosomes.

These results showed that unrepaired DSBs not only disrupt karyosome formation but also other NHK-1 dependent events. This suggests that suppression of NHK-1 activity plays wider roles in delaying meiotic progression in response to DSBs.

### The meiotic checkpoint suppresses NHK-1 activity to delay nuclear reorganisation in meiosis

These NHK-1 dependent events, disassembly of the synaptonemal complex, loading of condensin and karyosome formation, represent an important transition in oocyte nuclear organisation during meiosis. Temporally karyosome formation takes place at the transition between oogenesis stage 2 and 3 [26] and in fact our quantitative study of synaptonemal complex disassembly and condensin loading in wild-type meiosis (Figure 5B and 5D) indicated that the initiation of these other two NHK-1 dependent events also occurs between oogenesis stage 2 and 3. As these events depend on the presence of a functioning NHK-1 kinase [28], it suggests that NHK-1 is a key meiotic regulator of this important transition in nuclear organisation in oocytes.

It has long been known that activation of the meiotic recombination checkpoint disrupts karyosome formation, and additionally we show here that synaptonemal complex disassembly and condensin loading are delayed by the presence of unrepaired DSBs and an activated checkpoint. It has previously been shown that the meiotic checkpoint blocks oocyte polarisation by suppressing Gurken translation or localisation [16,17,23], but it was not previously known how the checkpoint affects karyosome formation or any other nuclear events in oocytes. Our study has shown that the meiotic checkpoint suppresses phosphorylation of an NHK-1 substrate, H2A, when DSBs are not repaired. Furthermore, we found that DSBs induced by X-rays suppress the kinase activity of NHK-1 in S2 cells. These results indicate that NHK-1 is a downstream effector of the meiotic recombination checkpoint, whose suppression is responsible for blocking karyosome formation and other meiotic events until DSBs are repaired.

Based on this evidence, we propose a model in which DSBs formed during recombination suppress the activity of the conserved kinase NHK-1 through the meiotic recombination checkpoint to delay oocyte nuclear reorganisation from a recombination to a post-recombination phase (Figure 6). Although the evidence is mostly genetic or cytological, all data are so far consistent with this model. Nevertheless, the model is likely to be too simplistic and to represent only a part of the whole picture. For example, we do not exclude the possibility that other checkpoint effectors are also involved in delaying meiotic progression. We hope that our proposed model will prompt further investigation to fully uncover how the meiotic checkpoint is linked to meiotic progression.

How does NHK-1 kinase control this critical transition in meiosis? Our previous study showed that NHK-1 directly controls karyosome formation through phosphorylation of BAF, a linker between the nuclear envelope and chromatin [31]. Phosphorylation of BAF by NHK-1 releases meiotic chromosomes from tethering at the nuclear envelope to allow karyosome formation. Expression of non-phosphorylatable BAF disrupts karyosome formation, but not synaptonemal complex disassembly or condensin loading (Figure S6). Therefore, NHK-1 appears to control two independent pathways during nuclear reorganisation. This is consistent with a recent study [36] showing that condensin is required for synaptonemal complex disassembly but not for karyosome formation. Karyosome formation and condensin loading are therefore likely to be two primary targets of NHK-1 activity.

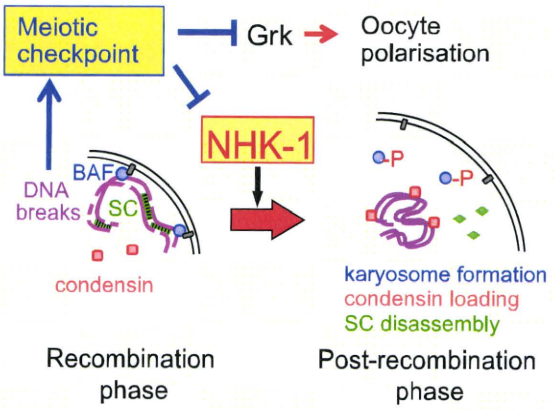


**Figure 6. A central role for NHK-1 kinase in meiotic progression.** NHK-1 promotes nuclear reorganisation from a recombination phase to a post-recombination phase, including karyosome formation, synaptonemal complex disassembly and condensin loading. NHK-1 directly phosphorylates BAF that anchors meiotic chromosomes to the nuclear envelope. DSBs activate the meiotic recombination checkpoint that suppresses NHK-1 kinase to prevent nuclear reorganisation.
doi:10.1371/journal.pgen.1001179.g006

Finally, this study in *Drosophila* is likely to have significant implications for our understanding of meiotic regulation at a molecular level in other organisms, since the processes we studied here are conserved among eukaryotes. The meiotic checkpoint that coordinates recombination events with meiotic progression is universally found across eukaryotes. Furthermore, NHK-1 is well conserved among animals, and karyosome-like clustering of meiotic chromosomes, as well as synaptonemal complex disassembly and condensin loading, is widely found in oocytes of various species including humans. In addition, this study has also suggested an involvement of NHK-1 in the DNA damage response during the mitotic cell cycle.

## Materials and Methods

### *Drosophila* genetics

Standard techniques of fly manipulation were followed [37]. All stocks were grown at 25°C on standard cornmeal media except in some case where females were matured at 18°C. General details of mutations, chromosome aberrations and common vectors can be found in [38] or at Flybase [39]. $w^{1118}$ was used as wild type. The following mutant alleles were used in this study: $nhk\text{-}1^{E24}$ and $nhk\text{-}1^{Z3\text{-}0437}$ analysed as a hemizygote over the deficiency *Df(3R)ro-80b* [29,28]; $spnA^{1}$ [13], $spnB^{1}$ [13] analysed as a hemizygote over the deficiency *Df(3R)red31* and $spnD^{2}$ [13] that were obtained from the Bloomington Drosophila Stock Centre; $vas^{4}$ [40]; $mnk^{p6}$ [21]. Flies containing both $spnA^{1}$ and $mnk^{p6}$ mutations were obtained by standard successive genetic crosses. BAF and non-phosphorylatable BAF-3A were expressed from pUASp-BAF and pUASp-BAF-3A transgenes using a maternal Gal4 driver (V2H) under the α-tubulin67C promotor, as previously described [31].

### Immunological and cytological techniques

Standard immunological techniques were used throughout [41]. *Drosophila* ovaries were immunostained essentially as described [42]. Briefly, ovaries were dissected from mature females in Robb's medium (100 mM HEPES, pH7.4, 55 mM sodium acetate, 40 mM potassium acetate, 100 mM sucrose, 10 mM glucose, 1.2 mM

$MgCl_2$, 1 mM $CaCl_2$) before being fixed in formaldehyde (8% paraformaldehyde, 100 mM potassium cacodylate, pH7.2, 100 mM sucrose, 40 mM potassium acetate, 10 mM sodium acetate, 10 mM EGTA). Following a blocking and permeabilization step (in PBS containing 10% foetal bovine serum and 1% Triton X-100), ovaries were successively incubated in primary and secondary antibody solutions before mounting on coverslips in mounting medium (85% glycerol, 2.5% propyl gallate). The primary antibodies used in this study were those against H2ApT119 [30] (1/200), γ-H2Av (this study; 1/100), H2A (Ab13923, Abcam; 1/250), Lamin [43] (1/250), C(3)G [44] (1/3000) and CAP-D2 [35] (1/5000). The antibody against γ-H2Av was generated by Eurogentec using a phospho-peptide (CQRKGNVILpSQAY-COOH), and differentially purified using the phospho-peptide and an equivalent non-phospho-peptide. The antibody gave punctate staining in oocyte nuclei during early oogenesis and in X-ray irradiated nuclei in S2 cells, but not during late oogenesis or non-irradiated S2 nuclei. Secondary antibodies conjugated with Cy3 or Alexa488 (Jackson Lab or Molecular Probes) were used at a 1/100 dilution. DNA was counterstained with DAPI (0.4 μg/ml; Sigma) or propidium iodide (2 μg/ml, Sigma). A series of 1 μm optical sections were taken using a Plan-Apochromat lens (63X, 1.4NA; Zeiss) attached to an Axiovert 200M (Zeiss) with a confocal scan head (LSM510meta; Zeiss) or to an Axioimager (Zeiss) with an LSM5 Exciter (Zeiss). A single mid-section of the oocyte nucleus has been presented. All digital images were imported to Photoshop (Adobe) and adjusted for brightness and contrast uniformly across entire fields.

### Expression of NHK-1-GFP in S2 cells and *in vitro* kinase assay

The culture and transfection of S2 cells were performed as previously described [45]. NHK-1-GFP under the metallothionein promoter was generated by a Gateway-based method (Invitrogen) and NHK-1(K77R)-GFP was made by site-directed mutagenesis. Stable cell lines were created through selection by inclusion of blasticidin in the culture medium. Untransfected S2 cells were used as a control. NHK1-GFP expression from the metallothionein promoter was induced by culturing in medium containing 0.7 mM copper sulfate for 72 h. Aliquotes of cells were adhered to coverlips coated with Concanavalin A for immunostaining for γ-H2Av and GFP. Cells, together with adhered cells, were irradiated with X-rays (1 Gy/minute) for 5 minutes. Subsequently, $2.5\times10^7$ cells were lysed in 500 μl of buffer (20 mM Tris pH 7.5, 150 mM NaCl, 5 mM EGTA, 1 mM DTT, 1 mM PMSF, Complete EDTA-free protease inhibitor cocktail (Roche)) supplemented with 10× Protein Phosphatase Inhibitor Cocktail 2 (Sigma).

The cleared lysate was then incubated with 5μl of mouse-anti-GFP antibody (3E6, Molecular Probes) for 1h at 4°C before the addition of 50 μl of 1:1 protein G beads (Invitrogen) in lysis buffer for 1h at 4°C. The beads were washed with the lysis buffer and kinase reaction buffer (10 mM HEPES pH 7.6, 50 mM KCl, 5 mM $MgCl_2$, Complete EDTA-free protease inhibitor cocktail (Roche)) supplemented with 10× Protein Phosphatase Inhibitor Cocktail 2 (Sigma).

In a typical kinase reaction, the suspension of beads and kinase buffer was mixed with 5 μCi of γ-[$^{32}$P]ATP (EasyTides, Perkin Elmer) and incubated at room temperature (20°C) for 60 min before the addition of 20 μl of 2× protein sample buffer. The samples were analyzed by SDS-PAGE, and dried gels were exposed to x-ray films (high performance autoradiography films, GE Healthcare).

### Karyosome image analysis

Analysis of karyosome morphology was performed for images of oocytes stained for lamin and DNA. For each series of images through an oocyte nucleus, the optical sections within which the karyosome was visible were determined. Of these, the mid-optical section was selected for analysis (or the lower of the middle two optical sections where this was the case), and the karyosome morphology categorised. Relative intensities of H2ApT119 or H2A signal on the karyosome in the oocyte nucleus were calculated using images of oocytes stained for H2ApT119 or H2A and DNA. As described above, the mid-optical section within which the karyosome was visible was selected for analysis. Using ImageJ software (NIH), the area corresponding to the karyosome was selected and the maximum H2ApT119 signal intensity on the karyosome was obtained and divided by that in surrounding follicle cell nuclei (an average of maximum signal intensity measurements in three nuclei at similar focal planes) after both intensities had been normalized by subtracting the background maximum signal intensity for a randomly selected area in the oocyte cytoplasm. Relative intensities of DNA staining signal on the karyosome were obtained using the same analysis method, and a measurement of H2ApT119 or H2A signal relative to DNA staining signal on the karyosome was made by dividing the two values for each image. We always compare samples processed in parallel or within a short time frame, as the exact values can vary over time due to a change in various factors including the conditions of the fixative and antibodies. Karyosome staining patterns for oocytes stained for C(3)G or CAP-D2 and counterstained for DNA were categorised as described in 'Results and Discussion' and Figure 5. A student t test or $\chi^2$ test was used for statistical analysis.

## Supporting Information

**Figure S1** Variation of karyosome defects in *nhk-1*, *spnA*, *spnB*, *spnD*, and *vas* mutants. (A) Three examples of karyosomes are shown for each mutant. Karyosomes in each mutant are always partially if not extensively localised at the edge of the oocyte nucleus. Similar karyosome morphology phenotypes are observable in *nhk-1* and all *spn* mutants, although the penetrance of the more severe phenotypes is variable between each mutant. Bar = 10 μm. (B) Karyosome morphology was categorised into 5 classes (from the left; spherical and detached from the nuclear membrane (NE), spherical and attached to the NE, deformed and attached to the NE, severely deformed and attached to the NE, deformed and detached from the NE).
Found at: doi:10.1371/journal.pgen.1001179.s001 (4.31 MB EPS)

**Figure S2** Delayed DSB repair was not detected in *nhk-1*$^{E24/Df}$ mutant oocytes. Oocytes at stage 5–7 from wild type, *spnA* and *nhk-1*$^{E24/Df}$ were immunostained for DNA and phospho-H2Av (γ-H2Av; which accumulates at DSB sites). No phospho-H2Av foci were observed in wild type indicating that DSBs are already repaired. Such foci were observed in a *spnA* mutant due to a failure of DSB repair during recombination. In the *nhk-1* mutant, no phospho-H2Av foci were observed indicating that DSBs were repaired. At least 6 karyosomes were examined. Bar = 10 μm.
Found at: doi:10.1371/journal.pgen.1001179.s002 (1.44 MB EPS)

**Figure S3** Suppression of H2A T119 phosphorylation by DSBs was not due to general karyosome abnormality or a reduction of H2A on chromosomes. (A) H2A T119 phosphorylation in wild-type, *spnA*$^1$ and *spnB*$^1$ *oocytes*. (B) H2A T119 phosphorylation in wild-type oocytes expressing wild-type BAF (wtBAF) and non-phosphorylatable BAF (BAF-3A) [31]. Ovaries at stage 5-7 were immunostained for H2ApT119 and DNA. Arrowheads indicate meiotic chromosomes in oocytes. Bar = 10 μm. (C) Ratios of signal intensities between phospho-H2A (H2ApT119) and DNA staining

in oocytes are shown with standard errors of the mean (SEM). The same oocytes used in Figure 2B were re-analysed. NHK-1 activity measured by H2A T119 phosphorylation was significantly reduced in *nhk-1* and *spn* mutant oocytes ($p<0.01$; marked with asterisks). (D) Ovaries at stage 5–7 were prepared from wild type, *spnA* and *spnD* as above except a phospho-independent anti-H2A antibody was used. (E) Ratios between H2A and DNA signals in oocytes were quantified as above. No significant differences were observed ($p>0.3$).
Found at: doi:10.1371/journal.pgen.1001179.s003 (6.24 MB EPS)

**Figure S4** Unrepaired DSBs suppress NHK-1 activity through the meiotic checkpoint. (A) H2A T119 phosphorylation in oocytes of wild type, *spnA* and *mnk spnA*. Ovaries at stage 5–7 were immunostained for H2ApT119 and DNA. Bar = 10 μm. (B) The H2ApT119 signal intensity on the chromosomes in oocytes was measured relative to that in follicle cells. The bars on the graph represent standard error of the mean (SEM). At least ten oocytes from each genotype were quantified. These samples were processed in parallel and compared only with each other, as exact values vary over time due to changes in factors including the conditions of the antibodies and fixative. NHK-1 activity measured by H2A T119 phosphorylation was significantly reduced in oocytes of a *spnA* mutant ($p<0.01$; marked with an asterisk), but not in those of an *mnk spnA* double mutant. Inactivation of the meiotic checkpoint rescued the suppression of NHK-1 activity in the presence of DSBs.
Found at: doi:10.1371/journal.pgen.1001179.s004 (5.91 MB EPS)

**Figure S5** The delay in synaptonemal complex disassembly in *spn* mutants was mediated by the meiotic recombination checkpoint. (A) Stage 6–8 ovaries from each genotype were immunostained for the synaptonemal complex protein C(3)G and DNA. Bar = 10 μm. (B) The C(3)G staining pattern at stage 6–8 was classified. The delay in synaptonemal complex disassembly in *spn* mutants was reversed by an *mnk* mutation that inactivates the meiotic checkpoint. A minimum of thirteen oocytes were counted. (C) DNA (left) and C(3)G (right) stainings in $nhk\text{-}1^{Z3\text{-}0437/Df}$, $mnk^{p6}$ $nhk\text{-}1^{Z3\text{-}0437/Df}$ and wild-type oocytes. Most oocytes in both mutants delay disassembly of filamentous C(3)G structures from chromosomes, and at late stages still have a residual fragmented appearance in the nucleoplasm (included in the "diffused" class; white bars in D). (D) The *mnk* mutation does not rescue the delay in disassembly of the synaptonemal complex in the *nhk-1* mutant. A minimum of ten oocytes were counted.
Found at: doi:10.1371/journal.pgen.1001179.s005 (4.62 MB EPS)

**Figure S6** Expression of non-phosphorylatable BAF does not block condensin loading and synaptonemal complex disassembly. Synaptonemal complex and condensin in wild-type oocytes expressing non-phosphorylatable BAF (BAF-3A) [31]. Ovaries at stage 5–7 were immunostained for the condensin subunit CAP-D2 or the synaptonemal complex protein C(3)G together with Lamin and DNA. Arrowheads indicate fragmented karyosome. Bar = 10 μm.
Found at: doi:10.1371/journal.pgen.1001179.s006 (1.04 MB EPS)

## Acknowledgments

We especially thank M. Heck, P. Fisher, M. Lilly, and T. Orr-Weaver for kindly providing antibodies and fly strains; K. Herbert and J. Burrage for assisting with the analysis and X-ray irradiation; and B. Loh for antibody testing and comments on the manuscript. We thank members of the Ohkura lab for discussion and support. We also thank the Bloomington stock centre and the DGRC for providing fly lines and plasmids.

## Author Contributions

Conceived and designed the experiments: OML MB HO. Performed the experiments: OML MB CFC. Analyzed the data: OML MB HO. Contributed reagents/materials/analysis tools: TI. Wrote the paper: OML HO.

## References

1. Keeney S, Giroux CN, Kleckner N (1997) Meiosis-specific DNA double-strand breaks are catalyzed by Spo11, a member of a widely conserved protein family. Cell 88: 375–384.
2. Dernburg AF, McDonald K, Moulder G, Barstead R, Dresser M, et al. (1998) Meiotic recombination in *C. elegans* initiates by a conserved mechanism and is dispensable for homologous chromosome synapsis. Cell 94: 387–398.
3. McKim KS, Hayashi-Hagihara A (1998) *mei-W68* in *Drosophila melanogaster* encodes a Spo11 homolog: evidence that the mechanism for initiating meiotic recombination is conserved. Genes Dev 12: 2932–2942.
4. Keeney S, Baudat F, Angeles M, Zhou ZH, Copeland NG, et al. (1999) A mouse homolog of the *Saccharomyces cerevisiae* meiotic recombination DNA transesterase Spo11p. Genomics 61: 170–182.
5. Page SL, Hawley RS (2004) The genetics and molecular biology of the synaptonemal complex. Annu Rev Cell Dev Biol 20: 525–558.
6. Bishop DK, Park D, Xu L, Kleckner N (1992) *DMC1*: a meiosis-specific yeast homolog of *E. coli recA* required for recombination, synaptonemal complex formation, and cell cycle progression. Cell 69: 439–456.
7. Gartner A, Milstein S, Ahmed S, Hodgkin J, Hengartner MO (2000) A conserved checkpoint pathway mediates DNA damage-induced apoptosis and cell cycle arrest in *C. elegans*. Mol Cell 5: 435–443.
8. Di Giacomo M, Barchi M, Baudat F, Edelmann W, Keeney S, et al. (2005) Distinct DNA-damage-dependent and -independent responses drive the loss of oocytes in recombination-defective mouse mutants. Proc Natl Acad Sci U S A 102: 737–742.
9. Hochwagen A, Amon A (2006) Checking your breaks: surveillance mechanisms of meiotic recombination. Curr Biol 16: R217–R228.
10. Hepworth SR, Friesen H, Segall J (1998) NDT80 and the meiotic recombination checkpoint regulate expression of middle sporulation-specific genes in *Saccharomyces cerevisiae*. Mol Cell Biol 18: 5750–5761.
11. Chu S, Herskowitz I (1998) Gametogenesis in yeast is regulated by a transcriptional cascade dependent on Ndt80. Mol Cell 1: 685–696.
12. Leu JY, Roeder GS (1999) The pachytene checkpoint in *S. cerevisiae* depends on Swe1-mediated phosphorylation of the cyclin-dependent kinase Cdc28. Mol Cell 4: 805–814.
13. Tearle R, Nüsslein-Volhard C (1987) Tübingen mutants stocklist. Drosophila Inform Service 66: 209–226.
14. Gonzalez-Reyes A, Elliott H, St Johnston D (1997) Oocyte determination and the origin of polarity in *Drosophila*: the role of the spindle genes. Development 124: 4927–4937.
15. Ghabrial A, Ray RP, Schüpbach T (1998) *okra* and *spindle-B* encode components of the RAD52 DNA repair pathway and affect meiosis and patterning in *Drosophila* oogenesis. Genes Dev 12: 2711–2723.
16. Styhler S, Nakamura A, Swan A, Suter B, Lasko P (1998) *vasa* is required for GURKEN accumulation in the oocyte, and is involved in oocyte differentiation and germline cyst development. Development 125: 1569–1578.
17. Ghabrial A, Schüpbach T (1999) Activation of a meiotic checkpoint regulates translation of Gurken during *Drosophila* oogenesis. Nat Cell Biol 1: 354–357.
18. Staeva-Vieira E, Yoo S, Lehmann R (2003) An essential role of DmRad51/SpnA in DNA repair and meiotic checkpoint control. EMBO J 22: 5863–5874.
19. Mehrotra S, McKim KS (2006) Temporal analysis of meiotic DNA double-strand break formation and repair in *Drosophila* females. PLoS Genet 2: e200. 10.1371/journal.pgen.0020200.
20. Chen Y, Pane A, Schüpbach T (2007) *cutoff* and *aubergine* mutations result in retrotransposon upregulation and checkpoint activation in *Drosophila*. Curr Biol 17: 637–642.
21. Klattenhoff C, Bratu DP, McGinnis-Schultz N, Koppetsch BS, Cook HA, et al. (2007) *Drosophila* rasiRNA pathway mutations disrupt embryonic axis specification through activation of an ATR/Chk2 DNA damage response. Dev Cell 12: 45–55.
22. Pane A, Wehr K, Schüpbach T (2007) *zucchini* and *squash* encode two putative nucleases required for rasiRNA production in the *Drosophila* germline. Dev Cell 12: 851–862.
23. Abdu U, Brodsky M, Schüpbach T (2002) Activation of a meiotic checkpoint during *Drosophila* oogenesis regulates the translation of Gurken through Chk2/Mnk. Curr Biol 12: 1645–1651.
24. Malone CD, Brennecke J, Dus M, Stark A, McCombie WR, et al. (2009) Specialized piRNA pathways act in germline and somatic tissues of the Drosophila ovary. Cell 137: 522–535.